

1 **Constraints of applying strontium isotope stratigraphy in coastal and shallow marine**  
2 **carbonates: insights from Lower Cretaceous carbonates deposited in an active tectonic**  
3 **setting (N Iberian Basin, Spain).**

4 Benito, M. Isabel<sup>a,b\*</sup>, Suarez-Gonzalez, Pablo<sup>a</sup>, Quijada, I. Emma<sup>c</sup>, Campos-Soto, Sonia<sup>a</sup>,  
5 Rodríguez-Martínez, Marta<sup>a</sup>

6

7 a Departamento de Geodinámica, Estratigrafía y Paleontología, Universidad Complutense de  
8 Madrid, 28040 Madrid, Spain.

9 b Instituto de Geociencias IGEO (UCM-CSIC).

10 c Departamento de Geología, Universidad de Oviedo. 33005 Oviedo, Spain

11 \*Corresponding author. Email: mibenito@ucm.es

12

13 **Abstract**

14           The Lower Cretaceous Leza Fm is an essentially carbonate unit deposited at the  
15 northernmost active margin of the Cameros Basin (N Spain) under an extensional tectonic  
16 regime. This unit is composed of freshwater, marine-influenced, marginal-marine and  
17 hypersaline marine carbonate facies, interbedded with variable amounts of alluvial deposits,  
18 mainly derived from the erosion of the Jurassic substrate.  $^{87}\text{Sr}/^{86}\text{Sr}$ ,  $\delta^{18}\text{O}$  and  $\delta^{13}\text{C}$  analyses  
19 were obtained from carbonate facies of the Eastern and Western sectors of the basin.  $\delta^{18}\text{O}$   
20 values follow the expected trend in both sectors: they are more negative (down to  $-7.9\text{‰}$ ) in  
21 freshwater carbonates and more positive (up to  $+2.8\text{‰}$ ) in marginal-marine to hypersaline  
22 facies. However, independently of the seawater or freshwater influence, in the Western Sector  
23 the  $^{87}\text{Sr}/^{86}\text{Sr}$  values (0.707373-0.707801) are significantly lower and closer to the published  
24 Lower Cretaceous seawater  $^{87}\text{Sr}/^{86}\text{Sr}$  ratios, than those of the Eastern Sector (0.707988-  
25 0.709033), where the overall marine influence was relatively high and the alluvial input low.  
26 These data strongly suggest that  $^{87}\text{Sr}/^{86}\text{Sr}$  ratios were mainly controlled by those of the riverine  
27 freshwater arriving to the coastal and marine areas after the weathering and erosion of the  
28 Jurassic carbonates or siliciclastic rocks, in the Western and Eastern sectors, respectively.  
29 Thus, data indicate that, in coastal and shallow marine carbonates the influence of the riverine  
30 water on the  $^{87}\text{Sr}/^{86}\text{Sr}$  ratios should be systematically evaluated. This is particularly necessary in  
31 active tectonic settings, where the uplifted areas are significantly prone to weathering and  
32 erosion and where alluvial fan systems commonly developed, eventually discharging into  
33 coastal and shallow marine areas.

34

35 **Keywords:** Cameros Basin, coastal wetlands, carbon and oxygen isotopes, water-rock  
36 interaction

37

38 **Resumen**

39 La Formación Leza es una unidad esencialmente carbonática del Cretácico Inferior  
40 depositada en el borde norte de la cuenca de Cameros (N de España) en un contexto tectónico  
41 extensional. Está formada por facies carbonáticas de agua dulce, con influencia marina,  
42 marinas marginales e hipersalinas, intercaladas con cantidades variables de depósitos  
43 aluviales, procedentes de la erosión del sustrato Jurásico de la cuenca. Se han obtenido datos  
44 de  $^{87}\text{Sr}/^{86}\text{Sr}$ ,  $\delta^{18}\text{O}$  y  $\delta^{13}\text{C}$  de las facies carbonáticas en las zonas Oriental y Occidental de la  
45 cuenca. Los valores de  $\delta^{18}\text{O}$  siguen la tendencia esperable en ambas zonas: son más  
46 negativos (hasta -7.9‰) en los carbonatos de agua dulce y más positivos (hasta +2.8‰) en las  
47 facies marinas marginales e hipersalinas. Sin embargo, independientemente de la influencia  
48 marina o de agua dulce, los valores de  $^{87}\text{Sr}/^{86}\text{Sr}$  de la zona Occidental (0.707373-0.707801)  
49 son significativamente inferiores y más próximos a los valores publicados para los carbonatos  
50 marinos del Cretácico Inferior, que los de la zona Oriental (0.707988-0.709033), donde la  
51 influencia marina fue, en general, relativamente mayor y el aporte aluvial menor. Estos  
52 resultados indican que las relaciones de  $^{87}\text{Sr}/^{86}\text{Sr}$  estuvieron controladas principalmente por las  
53 del agua dulce fluvial que llegaba a la zonas costeras y marinas tras la meteorización y erosión  
54 del sustrato Jurásico de la cuenca, carbonático en el Sector Occidental y siliciclástico en el  
55 Oriental, y sugieren que, para la interpretación de las relaciones de  $^{87}\text{Sr}/^{86}\text{Sr}$  en carbonatos  
56 costeros y marinos someros, sobre todo de aquéllos depositados en contextos tectónicamente  
57 activos, se debería evaluar sistemáticamente la influencia del agua dulce.

58

59 **Palabras clave:** Cuenca de Cameros, humedales costeros, isótopos de carbono y oxígeno,  
60 interacción agua-roca

61

## 62 1. Introduction

63 Strontium isotopes are commonly employed for dating and correlating marine  
64 carbonates and fossil shells based on the assumptions that the seawater  $^{87}\text{Sr}/^{86}\text{Sr}$  ratios of the  
65 world's oceans have changed through time, but they are, and have been, uniform for a given  
66 time (because its residence time is much greater than the time required for marine currents to  
67 mix waters) and that, in contrast to trace elements and C and O isotopes, there is no  
68 measurable fractionation of the Sr isotopes during precipitation of carbonates and fossil shells  
69 (Veizer and Compston 1974; Brass 1976; Burke et al. 1982; Banner 1995; Steuber and Veizer  
70 2002; McArthur et al. 2012). Accordingly, many curves reflecting the  $^{87}\text{Sr}/^{86}\text{Sr}$  variation of  
71 seawater through time have been published since the 70's, and they have been progressively  
72 more detailed and based on a larger number of samples for a given period of time (e.g. Veizer  
73 and Compston, 1974; Brass 1976; Burke et al. 1982; DePaolo and Ingram 1985; Koepnick et al.  
74 1988; Jones et al. 1994; McArthur 1994; McArthur et al. 1994; 2001; 2007; 2012; Veizer et al.  
75 1997; 1999; Jenkyns et al. 2002; Prokoph et al. 2008; Roveri et al. 2014; Korte and Ullmann  
76 2016; Reghizzi et al. 2017; Wierzbowski et al. 2017). Based on those curves, the strontium  
77 isotope stratigraphy (SIS) has become a powerful tool, used for dating and correlating marine  
78 carbonate sequences (including deep to shallow and normal to restricted environments), as well  
79 as for estimating the duration of stratigraphic gaps, biozones or Stages, for constraining the age  
80 of condensed levels and as climatic indicator (e.g. DePaolo and Ingram 1985; Miller et al. 1988;  
81 Hess et al. 1989; McArthur et al. 1992; 1993, 2000; Brasier et al. 1996; Bralower et al. 1997;  
82 Barbieri et al. 1998; Weedon and Jenkyns 1999; Azmy et al. 1999; Scasso et al. 2001; Ebneith  
83 et al. 2001; Steuber 2001; Price and Grocke 2002; Nieto et al. 2008; Frijia and Parente 2008;  
84 Bodin et al. 2009; Lugli et al. 2010; Boix et al. 2011; Wehmiller et al. 2012; Williamson et al.  
85 2012, Steuber and Schlüter 2012; Bonilla-Rodríguez et al. 2014, Frijia et al. 2015; Bover-Arnal  
86 et al. 2016; Caus et al. 2016; Zuo et al. 2018; Frau et al. 2018; Fan et al. 2020, among many  
87 others).

88 However,  $^{87}\text{Sr}/^{86}\text{Sr}$  values of the riverine and lacustrine freshwater may vary significantly  
89 because they depend on the Sr isotopic values of the rocks that are being weathered and  
90 eroded and on their  $^{87}\text{Rb}$  content, commonly high in silicate rocks, which, after its decay to  $^{87}\text{Sr}$ ,  
91 will significantly increase the  $^{87}\text{Sr}/^{86}\text{Sr}$  ratio (Faure 1977; Steuber et al. 1984; Banner 1995).

92 Because of that, some authors have attempted to distinguish between marine and non-marine  
93 environments based on the Sr isotopes (Schmitz et al. 1991; Hofer et al. 2013; Gierlowski-  
94 Kordesch and Cassle, 2015), and many other authors have studied and analysed the  
95 importance of fresh- and seawater mixing and its relevance on the  $^{87}\text{Sr}/^{86}\text{Sr}$  values in coastal to  
96 shallow marine areas, close to the mainland (Müller et al. 1990; Müller and Mueller 1991;  
97 Ingram and Sloan 1992; Andersson et al. 1992; Bryant et al. 1995; Banner 1995; Flecker et al.  
98 2002; Flecker and Ellam 2006; Lugli et al. 2010; Topper et al. 2011; Sessa et al. 2012; Topper  
99 and Meijer 2013; Roveri et al. 2014; Quijada et al. 2016a; Manzi et al. 2018; Meknassi et al.,  
100 2018; Roveri et al. 2019; Madhavaraju et al. 2020). In this sense, it has been argued by some  
101 authors that the seawater  $^{87}\text{Sr}/^{86}\text{Sr}$  ratio is rarely altered by freshwater inputs if salinities are  
102 maintained above 10 to 20‰ (Ingram and Sloan 1992; Bryant et al. 1995; McArthur et al.  
103 2012), although it has also been highlighted, even by the same authors, that small inputs of  
104 riverine waters may have significant effects on the  $^{87}\text{Sr}/^{86}\text{Sr}$  values of carbonate rocks and  
105 shells, and that it would be wise to evaluate whether the local riverine inputs have altered the  
106 seawater signals (Bryant et al. 1995; Banner 1995; McArthur et al. 2012; Meknassi et al., 2018)  
107 when analysing Sr isotopic compositions in coastal and shallow marine carbonates and shells.

108 In this study, we have attempted to evaluate this issue by analysing carbonates of the  
109 Leza Fm (Late Barremian-Early Aptian, Cameros Basin, N Spain), a coastal and essentially  
110 carbonate unit, deposited in the context of the Mesozoic Iberian Extensional System (Fig. 1).  
111 This unit is composed of freshwater, marine-influenced and marginal-marine carbonates,  
112 restricted marine carbonates and evaporites, and alluvial detrital deposits that mainly derive  
113 from the erosion of the uplifted Upper Jurassic substrate, which is essentially carbonate or  
114 essentially siliciclastic, depending of the sector of the basin (Durántez et al. 1982; Alonso and  
115 Mas 1990; Hernández-Samaniego et al. 1990; Ramirez Merino et al. 1990; Suarez-Gonzalez et  
116 al. 2013; 2015). Thus, the main aim of this work is to evaluate the influence of the riverine  
117 waters on the  $^{87}\text{Sr}/^{86}\text{Sr}$  ratios of carbonates deposited in the different depositional environments  
118 (from freshwater to marine and hypersaline) of the Leza Fm, and to evaluate the significance of  
119 the  $^{87}\text{Sr}/^{86}\text{Sr}$  ratios of the Jurassic substrate, weathered and eroded during deposition, in  
120 affecting the seawater  $^{87}\text{Sr}/^{86}\text{Sr}$  ratios.

## 121 **2. Geological setting and stratigraphic framework**

122           The Cameros Basin is the northernmost basin of the Mesozoic Iberian Extensional  
123 System (Fig. 1A-B). It was developed from the Tithonian to the Early Albian and records up to  
124 6,500 m of vertical thickness of sediments (Mas et al. 2011; Omodeo-Salé et al. 2014; 2015;  
125 Mas et al. in Martin-Chivelet et al. 2019). During the Eocene to Early Miocene, the Cameros  
126 Basin was tectonically inverted, leading to the development of the thrusts that now limit the  
127 Cameros structural unit to the north and south (Fig. 1B; Platt 1990; Casas-Sainz and Simón-  
128 Gómez 1992; Salas and Casas, 1993; Mas et al. 1993; 2011; Guimerà et al. 1995; Salas et a.,  
129 2011; Mas et al. in Martin-Chivelet et al., 2019).

130           The sedimentary record of the Cameros Basin comprises eight depositional sequences  
131 (DS) (Mas et al. 2002; 2011; Arribas et al. 2003; Fig. 1C), and is characterised by the overall  
132 and progressive migration of the depocenters of the successive DS to the N, which results in an  
133 onlapping geometry observed between the successive units and the underlying Jurassic and,  
134 locally Upper Triassic, substrate (Fig. 2A; Guiraud 1983; Mas et al. 1993; Suarez-Gonzalez et  
135 al. 2013; 2016a; Omodeo-Salé et al. 2014; Mas et al. in Martin-Chivelet et al. 2019). In general,  
136 the sedimentary record of the Cameros Basin is gently folded, and it is apparently unaffected by  
137 relevant internal deformation (Guiraud 1983; Guiraud and Seguret 1985; Mas et al. 1993;  
138 Omodeo-Salé et al. 2015); however, to the N and NE margins of the basin, where this study has  
139 been carried out, it has been interpreted that syn-sedimentary normal faults controlled the  
140 generation of the accommodation space and the thickness of some DS (Guiraud, 1983; Gómez-  
141 Fernández 1992; Quijada et al. 2013a; Suarez-Gonzalez et al. 2013; 2015; 2016a; Omodeo-  
142 Salé et al. 2014). Specifically, in the studied N and NE Cameros Basin, Suarez-Gonzalez et al.  
143 (2016a) have interpreted that small fault-limited tectonic depressions were formed during the  
144 Late Barremian-Early Aptian due to the interaction of the general extensional direction (mainly  
145 N-S) with the late-Variscan structure of the basement. Additionally, the irregular distribution of  
146 the Triassic evaporites (Keuper Facies), and its association with the onlap geometry of DS 1–7  
147 onto the Jurassic substrate and even onto the Keuper Facies (Fig. 2A), led Suárez-González et  
148 al. (2016a) to interpret a probable role of salt-tectonics on the sedimentation at the northern part  
149 of the basin.

150           The sedimentary infill of the basin includes continental and coastal siliciclastic,  
151 carbonate and evaporite deposits (Fig. 1C). In general, facies distribution along the basin shows

152 a proximal-distal trend: proximal continental and detrital facies are located to the W and SW; the  
153 distal facies, comprising coastal carbonates, mixed carbonate-siliciclastic or mixed carbonate-  
154 evaporite deposits, are located to the E and NE of the basin (Mas et al. 1993; 2002; 2011; 2019;  
155 Arribas et al. 2003; Quijada et al. 2013a, 2013b; 2014; 2016b; 2020; Suarez-Gonzalez et al.  
156 2013; 2014; 2015; Sacristán-Horcajada et al. 2015; 2016).

157 The syn-extensional record in the studied area, located at the northern and north-  
158 eastern margin of the Cameros Basin (Figs. 1B; 2A), comprises deposits of the Urbión and  
159 Enciso Groups (DS7; Late Barremian-Early Aptian in age) and of the Oliván Group (DS8; Late  
160 Aptian-Early Albian in age) (Figs. 1B-C; 2A; Mas et al. 1993; 2002; 2011;; Suarez-Gonzalez et  
161 al 2013; 2015; 2016b; Mas et al., in Martin-Chivelet et al. 2019). The Urbión Group is  
162 represented in the studied area by deposits of the Jubera Fm (Figs. 1C; 2A-B), which is  
163 composed of reddish conglomerate, sandstone and siliciclastic mudstone (*sensu* Friedman et  
164 al., 1992) and is interpreted as deposited in alluvial fan systems (Alonso and Mas 1993; Mas et  
165 al. 2002; 2011; Ochoa 2006; Suárez-González et al. 2013). The Enciso Group overlies and  
166 passes laterally to the Urbión Group (Fig. 1C). In the studied area, the lower part of the Enciso  
167 Group is represented by the Leza Fm, which overlies and passes laterally to the Jubera Fm,  
168 and is the focus of this study (Figs. 1C; 2A-B). The Leza Fm is essentially composed of  
169 carbonates, with variable marine influence and content of detrital deposits, and is interpreted as  
170 deposited in a coastal-wetland system (Suarez-Gonzalez et al. 2013; 2015). The rest of the  
171 Enciso Group, which overlie and pass laterally to deposits of the Leza Fm (Figs. 1C; 2A-B), is  
172 composed of mixed carbonate-siliciclastic deposits interpreted as deposited in siliciclastic-  
173 influenced lacustrine and palustrine systems (Mas et al. 1993; 2002; 2011). The Oliván Group is  
174 composed of reddish to greenish sandstone and siliciclastic mudstone deposited in fluvial and  
175 coastal systems (Mas et al. 2011; Mas et al., in Martin-Chivelet et al. 2019).

176 A relevant feature of the Jubera and Leza Fms is that their deposits show significant  
177 variations in their thickness, as they were deposited in the above-mentioned small tectonic  
178 depressions formed during the Late Barremian – Early Aptian by faulting of the basin substrate  
179 (Fig. 2A-B; Alonso and Mas 1993; Suarez-Gonzalez et al. 2013; 2015; 2016a). The substrate of  
180 the Cameros Basin is mainly composed of Jurassic, and locally Upper Triassic, rocks (Fig. 2A,  
181 see below for details), which underlie syn-extensional deposits through an important

182 unconformity (Alonso and Mas 1993; Mas et al. 1993; 2002; 2011; Benito et al., 2001; 2005;  
183 Benito and Mas, 2002; 2006). Erosion of the faulted substrate led to deposition of alluvial fan  
184 sediments throughout the Jubera Fm; in the Leza Fm, alluvial fan deposits were restricted to the  
185 margins of the depressions, and they changed laterally to carbonate coastal wetland sediments  
186 (Fig. 3; Suarez-Gonzalez et al. 2013; 2015). This coastal wetland system was composed of a  
187 mosaic of diverse and interrelated environments with influence of both fresh- and sea-water, the  
188 latter coming both from the North, from the Boreal Realm, and the South, from the Tethys Sea  
189 (Fig. 3; Suarez-Gonzalez et al., 2013).

190 Two main sectors are distinguished in the studied area, the Western and the Eastern  
191 (Figs. 2-3), which have important differences in the sedimentary features of both the Jurassic  
192 substrate and the syn-extensional Jubera and Leza Fms.

193 In the Western Sector, the substrate of the Jubera-Leza Fms comprises Upper Triassic  
194 to Upper Jurassic rocks (Fig. 2A-B; Suarez-Gonzalez et al. 2013; 2015; 2016a). The Triassic is  
195 composed of the Keuper Facies, which includes evaporites (gypsum), reddish siliciclastic  
196 mudstone and minor dolostone (Fig. 2A; Suarez-Gonzalez 2015; Suárez-González et al.,  
197 2016a). The Keuper facies are largely deformed, and their thickness varies significantly along  
198 the northern Cameros thrust (Fig. 2A). The Lower Jurassic is composed of approximately 150-  
199 200 m-thick marine limestone and/or dolostone, which were deposited in shallow to very  
200 shallow carbonate platforms (Mensink 1966; Bulard 1972; Ramírez-Merino et al. 1990;  
201 Hernández-Samaniego et al. 1990). The Middle Jurassic comprises approximately 300 m-thick  
202 marine limestone, including a thick Bathonian sequence (up to 150 m thick) mainly composed of  
203 oolitic deposits with minor siliciclastics, which were deposited in a shallow carbonate platform  
204 (Benke 1981; Benke et al. 1981; Wilde 1990; Ramírez-Merino et al. 1990; Hernández-  
205 Samaniego et al. 1990; García-Frank et al. 2008). The pre-extensional Upper Jurassic record  
206 (Oxfordian and Kimmeridgian) is composed of relatively thin shallow marine units (down to less  
207 than 50 m thick), which include abundant coral reef deposits of Kimmeridgian age and minor  
208 siliciclastic marine deposits (Benke et al. 1981; Alonso and Mas 1988; 1990; Errenst 1990;  
209 Benito and Mas 2006). The overlying syn-extensional sedimentary record of the Jubera and  
210 Leza Fms in the Western Sector, although highly variable, reaches up to approximately 500 m  
211 of thickness (Fig. 2B; Suarez-Gonzalez et al. 2013). In this sector, the detrital facies of both



212 units are mainly composed of carbonate clasts coming from the erosion of the different units of  
213 the Jurassic, mainly from the Bathonian to the Kimmeridgian units (Fig. 4A-B; Alonso and Mas  
214 1993; Ochoa 2006; Suarez-Gonzalez et al. 2013; 2015); moreover, in the Western Sector the  
215 overall detrital influence in the Leza Fm is higher than in the Eastern Sector (Suarez-Gonzalez  
216 et al., 2015; see below and details in Section 4).

217 In the Eastern Sector, the substrate of the Jubera-Leza Fms is composed of Upper  
218 Jurassic rocks (Figs. 2A-B; Suarez-Gonzalez et al. 2013; 2015). The Upper Triassic Keuper  
219 Facies (which include very scarce and local outcrops of volcanic to subvolcanic rocks, less than  
220 0.01 Km<sup>2</sup>) and the Lower and Middle Jurassic carbonate rocks are also observed in this sector,  
221 but they do not directly underlie the syn-extensional sedimentary record (Fig. 2A; Suarez-  
222 Gonzalez et al., 2016a) and, thus, they probably they did not crop out during sedimentation of  
223 the Jubera and Leza Fms. In the Eastern Sector, deposits from the Upper Triassic to the  
224 Bathonian are equivalent to those observed in the Western Sector (Mensink 1966; Bulard 1972;  
225 Durántez et al. 1982; Hernández-Samaniego et al. 1990). However, and in contrast to what is  
226 observed in the Western Sector, in the Eastern Sector the Callovian to Kimmeridgian  
227 sedimentary record is mainly composed of marine sandy limestone, sandstone and quartzite  
228 conglomerates, which reach up to around 150 m (Benke 1981; Benke et al. 1981; Durántez et  
229 al. 1982; Alonso and Mas 1988; 1990; Wilde 1990; Hernández-Samaniego et al. 1990; García-  
230 Frank et al. 2008). The syn-extensional sedimentary record of the Jubera and Leza Fms in the  
231 Eastern Sector, although also variable, is overall thinner (up to 300 m) than in the Western  
232 Sector (Fig. 2B; Alonso and Mas 1993; Suarez-Gonzalez et al. 2013; 2015); moreover in the  
233 Eastern Sector, detrital deposits of both the Jubera and Leza Fms came from the erosion of the  
234 Callovian and the Upper Jurassic units, which are mainly composed of quartzite conglomerate  
235 and sandstone, with minor detrital carbonate fraction (Fig. 4C-D; Suarez-Gonzalez et al. 2015).  
236 Additionally, the overall detrital content of the Leza Fm deposits is lower in the Eastern Sector  
237 than in the Western Sector (see details in Section 4).

### 238 **3. Materials and methods**

239 Two selected stratigraphic sections of the Leza Fm, one from the Eastern Sector of the  
240 northern Cameros Basin (Préjano section), and another one from the Western Sector (the Leza  
241 River section) have been used for this study (Figs. 2, 5). A total of 341 rock samples from the

242 Leza Fm (214 limestone or marly limestone, 49 dolostone, 57 sandstone or sandy limestone, 21  
243 conglomerate) were collected for laboratory studies (see Suarez-Gonzalez, 2015 for details  
244 regarding the facies and samples). For each sample, a polished and uncovered thin section was  
245 prepared to 30  $\mu\text{m}$  thickness for petrographic analysis utilizing standard petrographic  
246 techniques and cathodoluminescence petrography. For 75 samples, a polished 150-200  $\mu\text{m}$   
247 thick section, matching the 30  $\mu\text{m}$  thin section, was prepared for isotopic analyses.  
248 Cathodoluminescence (CL) examination was carried out using a Technosyn® cold  
249 cathodoluminescence unit operating at 20-25 kV with 300-400  $\mu\text{A}$  beam current. Following  
250 examination with CL, thin sections were stained with Alizarin Red S and potassium ferricyanide  
251 (Dickson, 1966) for identification of carbonate minerals.

252 After petrographic examination and staining, well-preserved micritic or dolomicritic  
253 samples (samples displaying mudstone to wackestone texture *sensu* Dunham, 1962), lacking  
254 detrital input and petrographic evidence of diagenetic alteration, were selected for isotope  
255 analyses and microsampled directly from thick sections using a microscope-mounted drilling  
256 system, using 0.3 mm in diameter dental burs. When possible, approximately 20 mg of  
257 powdered samples were obtained, from which 100-150  $\mu\text{g}$  were used for C and O isotopic  
258 analyses, and the rest for  $^{87}\text{Sr}/^{86}\text{Sr}$  determinations.

259 62 analyses for  $\delta^{13}\text{C}$  and  $\delta^{18}\text{O}$  determinations were performed in the Stable Isotope  
260 Laboratory at the University of Michigan. Sample powders reacted at 73  $^{\circ}\text{C}$  during 6 and 12  
261 minutes (for calcite and dolomite, respectively) in an automated carbonate reaction system  
262 (CarboKiel-IV) coupled directly to the inlet of a Thermo MAT 253 gas ratio mass spectrometer.  
263 Isotopic ratios were corrected for  $^{17}\text{O}$  contribution and are reported in per mil notation relative to  
264 the VPDB standard. Values were calibrated utilizing NBS 19 as the primary standard, and  
265 analytical precision was monitored by daily analysis of NBS powdered carbonate standards.  
266 Precision was better than 0.1 ‰ for both  $\delta^{13}\text{C}$  and  $\delta^{18}\text{O}$  measurements.

267 58  $^{87}\text{Sr}/^{86}\text{Sr}$  ratios were determined on an automated multicollector TIMS-Phoenix®  
268 mass spectrometer at the Geochronology and Isotope Geochemistry Centre of the  
269 Complutense University of Madrid. Carbonate powder was dissolved in 5 ml of 0.5M acetic acid.  
270 Once dried, 1 ml of 3M  $\text{HNO}_3$  (Merk-Suprapur™) was added to the sample and dried again.

271 3ml of 3M HNO<sub>3</sub> (Merk-Suprapur™) were then added to the samples, which were  
272 subsequently centrifuged at 4000 r.p.m. during 10 minutes, in order to eliminate the solid  
273 residue (clay minerals, quartz, etc). For the Sr chromatographic separation, an extraction resin  
274 SrResin™ (Trisken International) was employed. The Sr was recovered with 0.05M HNO<sub>3</sub> as  
275 eluent. The fraction in which Sr was concentrated was recovered and dried for analysing in the  
276 mass spectrometer. Sr analyses have been corrected for possible interference of <sup>87</sup>Rb and they  
277 have been normalized to the value <sup>88</sup>Sr/<sup>86</sup>Sr=0.1194. Analytical precision was monitored by  
278 analysis of the NBS 987 standard (the mean value obtained for 7 samples were 0.710247; 2σ=  
279 0.000008). Analytical uncertainties (referred to 2σ) were 0.01% for <sup>87</sup>Sr/<sup>86</sup>Sr ratios. Blanks of Sr  
280 preparations were lower than 0.05 ng/ml. The standard error for each sample was equal to or  
281 lower than 3.

#### 282 **4. Results: The sedimentary record and isotopes of the Leza Fm.**

283 The Leza Fm is a predominantly carbonate coastal unit, which has variable content of  
284 detrital sediment and also shows a general trend of upwards increase in marine influence in  
285 both the Eastern and Western sectors (Fig. 5; see detailed facies descriptions and  
286 interpretations in Suarez-Gonzalez et al. 2013; 2014; 2015; 2016b; 2019). According to these  
287 authors, tectonic activity caused significant variations in subsidence and thickness the unit  
288 (which ranges from 20 m to 280 m) and in the lateral distribution of its facies, which include a  
289 wide variety of interrelated deposits (Fig. 3), grouped into five facies associations (FA, Figs. 5-  
290 6):

291 The alluvial fan FA is characterised by conglomerates and sandstones. As pointed out  
292 above (Section 2), in both the Eastern and the Western sectors, the main components of these  
293 facies are lithoclasts of the Middle and Upper Jurassic (Bathonian to Kimmeridgian) rocks of the  
294 basin substrate, which are mainly marine sandstone and quartzite conglomerates with minor  
295 limestone in the Eastern Sector, and marine limestone in the Western Sector (Fig. 4). Deposits  
296 of the alluvial fan FA are interbedded with freshwater to shallow marine carbonate deposits and,  
297 in the Eastern Sector, also with hypersaline marine dolostone, which are described below (Figs.  
298 5-6).

299            The freshwater and the marine-influenced limestone FAs are both characterised by  
300 black and fetid limestones and, less commonly, by marls, which are widespread in both sectors  
301 (Figs. 5; 6A-D). Abundant biota is observed in both FAs, including charophytes (in the  
302 freshwater FA; Fig. 6A-B), dasycladales (in the marine-influenced FA; Fig. 6C-D), ostracods,  
303 gastropods and vertebrate remains. Microbialites (oncoids, skeletal stromatolites and  
304 thrombolites) are also observed (Suarez-Gonzalez et al., 2019). Both freshwater and marine-  
305 influenced limestone FAs are generally arranged in thickening-upwards sequences up to 4 m  
306 thick, with abundant desiccation and edaphic features at their top (Figs. 5, 6A, C), and are  
307 interpreted as deposited in shallow water-bodies with diverse salinities, from fresh to near-  
308 marine, which underwent periods of desiccation and inundation, and were surrounded by  
309 vegetated areas (Suarez-Gonzalez et al. 2015). Thus, both FAs are sedimentologically  
310 equivalent, differing only in the influence of seawater and their palaeontological content.  
311 Lithoclasts of Jurassic rocks may occur within these limestone beds, indicating lateral  
312 association with the alluvial fan palaeoenvironments and suggesting that the source of  
313 freshwater to the water bodies was related to the weathering and erosion of the Jurassic  
314 substrate of the basin (Suarez-Gonzalez et al. 2013; 2015).

315            Regarding isotopic compositions, freshwater limestone yields  $\delta^{18}\text{O}$  values of -7.9 to -  
316 5.8‰ in the Eastern Sector and of -6.5 to -4.3‰ in the Western Sector;  $\delta^{13}\text{C}$  values range  
317 between -5.2 and -0.4‰ in the Eastern Sector and between -8.0 and -2.6‰ in the Western  
318 Sector;  $^{87}\text{Sr}/^{86}\text{Sr}$  ratios ranges between 0.708785 and 0.707988 in the Eastern Sector and  
319 between 0.707373 and 0.707719 in the Western Sector (Figs. 5, 7; Table 1 of Supplementary  
320 material).

321            Marine-influenced limestone yields  $\delta^{18}\text{O}$  values of -5.4 to -5.6‰ in the Eastern Sector  
322 and of -2.1 to -4.8‰ in the Western Sector;  $\delta^{13}\text{C}$  values range between -1.7 and -5.9‰ in the  
323 Eastern Sector and between -3.5 and -4.9‰ in the Western Sector;  $^{87}\text{Sr}/^{86}\text{Sr}$  ratios in the  
324 Western Sector range between 0.707597 and 0.707801 (Figs. 5, 7; Table 1 of Supplementary  
325 material). It was not possible to obtain enough micritic carbonate powder for performing Sr  
326 isotopes in thick sections of this FA in the Eastern Sector, because of the abundance of calcite  
327 cement filling intra- and interparticle primary porosity, which could have altered the Sr isotopic  
328 values of depositional (micritic) carbonate.

329            The marginal-marine carbonate FA (Fig. 6E-F) is characterised by grey limestone or  
330 dolostone, which are slightly different in the Eastern and in the Western sectors. In the Eastern  
331 Sector, these deposits are characterised by alternation of oolitic and micritic dolostone  
332 containing abundant ostracods, miliolid foraminifers and agglutinated stromatolites (Suarez-  
333 Gonzalez et al., 2014; 2016b; 2019), which displays flaser, wavy and lenticular bedding and  
334 subaerial exposure features. In the Western Sector, this FA consists of grey limestone, either  
335 bioclastic (containing ostracods, miliolid foraminifers and gastropods) or micritic, displaying  
336 commonly fenestral porosity and desiccation features. Facies in both sectors are interpreted as  
337 deposited in shallow marginal-marine areas affected by tides. This FA was dominated by  
338 seawater, with salinities mostly higher than in the marine-influenced FA, but still probably  
339 variable, temporarily decreasing due to freshwater influence (mainly in the Western Sector) or  
340 increasing, due to evaporation (in the Eastern Sector, see next FA), which in turn, favored early  
341 dolomite precipitation (Suarez-Gonzalez et al. 2014; 2015; 2016b; 2019), as observed in recent  
342 coastal carbonate settings where syn-depositional dolomite commonly precipitates (e.g. Tucker  
343 and Wright, 1990; Warren, 2016 and references therein).

344            In the Eastern Sector, marginal-marine dolostone of this FA yields  $\delta^{18}\text{O}$  values of -1.3 to  
345 +0.6‰,  $\delta^{13}\text{C}$  values of -6.7 to -1.8‰ and  $^{87}\text{Sr}/^{86}\text{Sr}$  ratios of 0.708302 to 0.708978. In the  
346 Western Sector, marginal-marine limestone of this FA yields  $\delta^{18}\text{O}$  values of -4.0 to -1.1‰,  $\delta^{13}\text{C}$   
347 values of -4.8 to -1.7‰ and  $^{87}\text{Sr}/^{86}\text{Sr}$  ratios of 0.707679 to 0.707761 (Figs. 5, 7; Table 1 of  
348 Supplementary material).

349            The hypersaline dolomite-evaporite FA (Fig. 6 G-H) is only observed in the Eastern  
350 Sector, where it is laterally associated with deposits of the marginal-marine FA (Figs. 3; 5). This  
351 FA is characterised by laminated dolomicritic deposits, containing rare ostracods and  
352 foraminifers, abundant pseudomorphs after gypsum and anhydrite, desiccation features and,  
353 locally, micritic-evaporitic stromatolites. The dolomite-evaporite FA is interpreted as deposited in  
354 very shallow and restricted hypersaline marine areas, which reached high salinity through  
355 evaporation (Suarez-Gonzalez et al. 2013; 2015; 2019).

356            Dolostone of this FA yields  $\delta^{18}\text{O}$  values of -1.0 to +2.8‰,  $\delta^{13}\text{C}$  values of -8.2 to -1.3‰  
357 and  $^{87}\text{Sr}/^{86}\text{Sr}$  ratios of 0.708304 to 0.709033 (Figs. 5, 7; Table 1 of Supplementary material).

358 **5. Discussion: Constraints of applying strontium isotope stratigraphy in coastal and**  
359 **shallow marine carbonates**

360 Isotopic data obtained from carbonates of the different FA of the Leza Fm in both  
361 studied sectors are apparently contradictory. As discussed below, the  $\delta^{18}\text{O}$  values reflect the  
362 sedimentary palaeoenvironment and the nature of the waters from which they precipitated,  
363 however, the  $^{87}\text{Sr}/^{86}\text{Sr}$  values reflect the strong influence of the riverine waters, which may have  
364 had a wide range of Sr isotope compositions, depending on the nature of rocks that were being  
365 weathered and eroded during deposition.

366  $\delta^{18}\text{O}$  values obtained from carbonates of the different FA, in both the Eastern and the  
367 Western sectors, are consistent with carbonate precipitation from fresh- to marine and even  
368 hypersaline waters. Freshwater limestone in both sectors shows the lowest  $\delta^{18}\text{O}$  values.  $\delta^{18}\text{O}$   
369 values progressively increase in marine-influenced limestone, in marginal-marine limestone (in  
370 the Western Sector) and dolostone (in the Eastern Sector) and in hypersaline dolostone (Figs.  
371 5, 7A-B). According to Prokoph et al. (2008), the oxygen isotopic composition of the Upper  
372 Barremian-Lower Aptian marine limestone and calcitic fossils deposited in low latitude (as that  
373 of the Iberian Plate for that time, e.g. Masse et al. 2000) ranged approximately between  $-2.8$   
374 and  $-0.4\text{‰}$  (Figs. 5, 7A-B). In the case of the Leza Fm,  $\delta^{18}\text{O}$  values of marginal-marine  
375 limestone of the Western Sector range between  $-4.0$  and  $-1.1\text{‰}$ , which are close to or in the  
376 range of the published marine values by Prokoph et al. (2008) (Figs. 5, 7A-B). In the Eastern  
377 Sector,  $\delta^{18}\text{O}$  values of marginal-marine dolostone range between  $-1.3$  to  $+0.6\text{‰}$ , being heavier  
378 than those of the marginal-marine limestone of the Western Sector, but also mostly in the range  
379 of the published marine values (Fig. 7A-B). The heavier  $\delta^{18}\text{O}$  values in dolostone (the mean  
380  $\delta^{18}\text{O}$  value of marginal marine dolostone is  $-0.31\text{‰}$  whereas the mean  $\delta^{18}\text{O}$  value of marginal  
381 marine limestone is  $-2.95\text{‰}$ ; Table 1 of supplementary material) are consistent with the  
382 difference between the water-calcite and the water-dolomite fractionation factors for a given  
383 temperature, which results in dolomite  $\delta^{18}\text{O}$  values of  $\sim 3\text{‰}$  heavier than those of the calcite  
384 precipitating from the same water and at the same temperature (Fritz and Smith 1970;  
385 Friedmann and O'Neil 1977; McKenzie 1981; Tucker and Wright 1990; Arenas et al., 1997).  
386 Freshwater limestone, as expected, shows more negative  $\delta^{18}\text{O}$  values, which are in the range of

387 carbonates precipitated from meteoric freshwater at low latitudes (e.g. Hudson 1977; Allan and  
388 Matthews 1982; Lohmann 1987; James and Choquette 1990; Tucker and Wright 1990). Marine-  
389 influenced limestone has  $\delta^{18}\text{O}$  values ranging between the marine and freshwater limestones,  
390 which would be derived from the mixing of sea- and freshwater at different proportions (e.g.  
391 Frank and Lohmann 1995). Dolostone of hypersaline facies has the heaviest  $\delta^{18}\text{O}$  values,  
392 ranging from -1.0 to +2.8‰. These values are in the range of the  $\delta^{18}\text{O}$  values obtained from  
393 dolomites precipitated in Cenozoic and recent coastal sabkhas undergoing intense evaporation  
394 (e.g. Tucker and Wright 1990; Arenas et al., 1997; Warren 2016, and references therein).

395         Regarding the C isotopic compositions, Prokoph et al. (2008) estimated  $\delta^{13}\text{C}$  values  
396 ranging approximately between +0.8 and +3.4‰ for marine limestone and calcitic fossils  
397 deposited in low latitude during the Late Barremian-Early Aptian.  $\delta^{13}\text{C}$  values of all analysed  
398 carbonates of the Leza Fm, however, are largely variable and more negative than those  
399 published for marine carbonates (Fig. 7A). This shift to lighter values would have been caused  
400 by the incorporation of  $^{12}\text{C}$  into calcite and dolomite, which could have derived from the  
401 oxidation of organic matter, commonly soil-derived (Allan and Matthews 1977; 1982; Lohmann  
402 1987; Tucker and Wright 1990; Leng and Marshall, 2004), and/or from bacterial sulphate  
403 reduction, as observed in some modern coastal sabkhas (Tucker and Wright 1990; Warren  
404 2016 and references therein). In fact, the combination of relatively invariant  $\delta^{18}\text{O}$  values with  
405 highly variable and negative  $\delta^{13}\text{C}$  values is a common trend in meteoric or in transitional marine-  
406 to-meteoric systems (Lohmann, 1987; James and Choquette, 1990).

407          $^{87}\text{Sr}/^{86}\text{Sr}$  ratios, as pointed out in the introduction, are commonly employed for dating  
408 and correlating marine carbonates (strontium isotope stratigraphy, SIS; McArthur, 1994; Veizer  
409 et al. 1997, 1999; Prokoph et al., 2008; McArthur et al., 2012, among many others) and,  
410 according to published data (Jones et al., 1994; McArthur et al., 2001; 2012; Prokoph et al.,  
411 2008), the  $^{87}\text{Sr}/^{86}\text{Sr}$  values of Upper Barremian-Lower Aptian marine carbonates approximately  
412 range between 0.7073 and 0.7075 (Figs. 5, 7C). However, and in contrast to what occurs with  
413 the O isotopic compositions,  $^{87}\text{Sr}/^{86}\text{Sr}$  data of the Leza Fm carbonates do not show the  
414 expected trend according to their different depositional palaeoenvironments in none of the  
415 studied sectors; moreover, the  $^{87}\text{Sr}/^{86}\text{Sr}$  ratios obtained in the Eastern and Western sectors are

416 significantly different (Figs. 5, 7C). In the Eastern Sector, the  $^{87}\text{Sr}/^{86}\text{Sr}$  ratios are higher (more  
417 radiogenic) than those expected for Upper Barremian-Lower Aptian marine carbonates.  
418 Additionally, it is also significant that all the analysed carbonates, regardless of their fresh-,  
419 marine- or hypersaline-water origin, show similar range of  $^{87}\text{Sr}/^{86}\text{Sr}$  values in each sector (more  
420 radiogenic in the Eastern Sector and less radiogenic in the Western Sector), despite  $\delta^{18}\text{O}$   
421 values being different according to their depositional palaeoenvironments (Fig. 7B-C). It could  
422 be argued that the Sr isotopic compositions, which are similar in all the carbonates of each  
423 sector, but different in the Eastern and in the Western sectors (Figs. 5, 7C), could be derived  
424 from diagenetic alteration. However, powder samples were carefully obtained from the areas of  
425 thick sections of samples with no evidences of diagenetic alteration; furthermore, it is important  
426 to note that, if the Sr isotopic ratios would have been altered by diagenetic fluids, changes in the  
427 oxygen isotopic compositions would be also expected, because the  $\delta^{18}\text{O}$  of carbonates depends  
428 on the  $\delta^{18}\text{O}$  of the waters from which they precipitate (a diagenetic fluid, if alteration had  
429 occurred) and on temperature (e.g. Fritz and Smith 1970; Friedmann and O'Neil 1977; Banner  
430 1995). However, the  $\delta^{18}\text{O}$  values are in accordance with the different palaeoenvironmental  
431 conditions where carbonates of the different FAs were formed, thus indicating the absence of  
432 significant diagenetic modification of the original isotopic signature.

433         Therefore, it is interpreted that the Sr isotopic values of carbonates of the Leza Fm are  
434 largely derived from  $^{87}\text{Sr}/^{86}\text{Sr}$  compositions of the riverine freshwaters that discharged into the  
435 coastal and shallow marine areas after weathering and eroding the faulted and exposed marine  
436 Jurassic rocks of the substrate. In the Eastern Sector, the eroded Middle to Upper Jurassic  
437 substrate, is mainly siliciclastic (e.g. Durántez et al. 1982; Hernández-Samaniego et al., 1990;  
438 see Section 4 for detail). In this regard, riverine waters may have a wide range of  $^{87}\text{Sr}/^{86}\text{Sr}$   
439 values, but if they have weathered and eroded Rb-rich silicate rocks (such as granite, gneiss  
440 and siliciclastic sedimentary rocks), their  $^{87}\text{Sr}/^{86}\text{Sr}$  values are commonly higher than those  
441 estimated for the Phanerozoic seawater (Faure 1977; Stueber et al. 1984; 1987; Banner 1995).  
442 In that case, even small inputs of riverine waters into the sea may have significant effects on the  
443  $^{87}\text{Sr}/^{86}\text{Sr}$  values of the resulting mixed water, which may increase significantly (Banner 1995,  
444 Bryant et al. 1995; McArthur et al., 2012; Meknassi et al., 2018). Thus, in the Eastern Sector,  
445 where essentially siliciclastic Jurassic rocks were being weathered and eroded, the more



446 radiogenic  $^{87}\text{Sr}/^{86}\text{Sr}$  values of the riverine freshwater would have significantly contributed to  
447 increase the marine  $^{87}\text{Sr}/^{86}\text{Sr}$  values of carbonates of the Leza Fm, while the oxygen isotopic  
448 compositions reflect their formation in the different freshwater to marine and hypersaline  
449 depositional palaeoenvironments (Fig. 7B-C).

450 In the Western Sector, however, the  $^{87}\text{Sr}/^{86}\text{Sr}$  values of freshwater to marginal-marine  
451 limestone are lower and closer to the published data of the Upper Barremian-Lower Aptian  
452 marine carbonates than those of the Eastern Sector, even though the overall marine influence  
453 in the Western Sector was lower than in the Eastern Sector (Figs. 5, 7C). In fact, in the Western  
454 Sector, the freshwater limestone shows  $^{87}\text{Sr}/^{86}\text{Sr}$  values closer to the Upper Barremian-Lower  
455 Aptian marine Sr isotopic values than those of the marginal-marine limestone, although the  $\delta^{18}\text{O}$   
456 values record the expected trend, consistent with their depositional environment (more negative  
457 in freshwater than in marginal marine carbonates) (Figs. 5, 7B-C, see above). These  
458 contradictory data may be explained if the following facts are considered: 1) in the Western  
459 Sector, the substrate that was being eroded was mainly composed of Lower to Upper Jurassic  
460 carbonates (e.g. Ramírez-Merino et al. 1990; Hernández-Samaniego et al. 1990; see section 4);  
461 2) the  $^{87}\text{Sr}/^{86}\text{Sr}$  ratios of the Jurassic marine carbonates range between  $\sim 0.7068$  and  $\sim 0.7077$   
462 (Jones et al. 1994; MacArthur 2001; Prokoph et al. 2008; MacArthur et al. 2012); 3) the range of  
463 the Jurassic Sr isotopic values, in turn, includes the range of  $^{87}\text{Sr}/^{86}\text{Sr}$  values from the Late  
464 Barremian to Early Aptian (Figs. 5, 7C). In this sense, and similarly to what occurs when  
465 weathering Rb-rich silicate rocks, previous authors have interpreted that meteoric waters and  
466 brines that interact with marine carbonates may inherit Sr isotope compositions that are  
467 diagnostic of the age of the carbonates (e.g. Müller et al. 1990; Müller and Mueller 1991; Banner  
468 et al. 1994; Banner 1995). Thus, in the Western Sector, the riverine freshwater would have had  
469 less radiogenic  $^{87}\text{Sr}/^{86}\text{Sr}$  values compared to those in the Eastern Sector, because Jurassic  
470 carbonates were being weathered and eroded, in contrast to the Eastern Sector, where the  
471 Jurassic substrate was mainly siliciclastic. Thus, in the Western Sector, when riverine and  
472 seawater mixed, both with similar Sr isotopic compositions, the resulting water would have  
473 similar Sr isotope ratio than that of both end members, leading to freshwater and marine  
474 carbonates having similar Sr isotopic ratios, but different  $\delta^{18}\text{O}$  values, depending on their

475 depositional environment, and even leading to freshwater carbonates showing  $^{87}\text{Sr}/^{86}\text{Sr}$  values  
476 within the range of the Late Barremian-Early Aptian values (Figs. 5, 7B-C).

477 In this regard, Bryant et al. (1995) made a two-component mixing model to calculate the  
478  $^{87}\text{Sr}/^{86}\text{Sr}$  of waters of different salinities and tested it with analyses performed in molluscs from  
479 estuaries of the Mississippi Sound and coastal Florida. On the one hand, these authors found  
480 out that both, their model results and analyses, suggested that even in the most marginal-  
481 marine systems the freshwater flux did not have a measurable influence until the salinity was  
482 very low (10 ppt or less), and these findings have been used for interpreting that “*when rivers*  
483 *locally lower the salinity of seawater, marine  $^{87}\text{Sr}/^{86}\text{Sr}$  is rarely altered at salinities above 20 psu*”  
484 (McArthur et al. 2012; note that psu is equivalent to g/kg or ‰). Nevertheless, Bryant et al.  
485 (1995) also pointed out that carbonates precipitating in estuarine settings not always record the  
486 global marine  $^{87}\text{Sr}/^{86}\text{Sr}$  value because, once the marine signature is affected by freshwater  
487 input,  $^{87}\text{Sr}/^{86}\text{Sr}$  seawater values change rapidly, leading McArthur et al. (2012) to highlight that  
488 “*when dating coastal and shallow water faunas, it is wise to establish that the local riverine*  
489 *inputs did not alter the  $^{87}\text{Sr}/^{86}\text{Sr}$  of seawater in the depositional environment.*”. More recently,  
490 Meknassi et al. (2018) have analysed  $^{87}\text{Sr}/^{86}\text{Sr}$  values from modern marine carbonate skeletons  
491 (bivalves, gastropods, cephalopods, chitons, and calcifying algae) collected in coastal settings  
492 worldwide and have found out that epibenthic and eurytopic organisms, such as bivalves and  
493 gastropods, from coastal domains with water mass restriction, low salinity or strong continental  
494 supplies, may display slight to considerable offsets compared to the  $^{87}\text{Sr}/^{86}\text{Sr}$  values of modern  
495 seawater. Based on their data, these authors calculated that “*only 10%, 33%, and 52% of the*  
496 *published Phanerozoic  $^{87}\text{Sr}/^{86}\text{Sr}$  curve can provide time calibration with respective accuracies of*  
497  *$\pm 1$ ,  $\pm 2$  and  $\pm 3$  m.y., hence obscuring most dating at the scale of the shorter Phanerozoic*  
498 *stages*”.

499 In the Leza Fm, our data strongly support that the  $^{87}\text{Sr}/^{86}\text{Sr}$  ratios of all carbonates  
500 (freshwater, marine-influenced, marginal-marine, and hypersaline) were, not only affected, but  
501 mainly controlled by the Sr ratios of the riverine freshwater, which discharged into the coastal  
502 and marine areas after weathering and eroding the carbonate or siliciclastic Jurassic substrate  
503 of the basin. Interestingly, this strong influence of freshwater Sr isotopic values is observed  
504 even without petrographic evidence of detrital input in the analysed carbonate samples, and

505 even though the  $\delta^{18}\text{O}$  values of carbonates are coherent with their formation from fresh- to  
506 marine and hypersaline waters. Nevertheless, it is important to highlight that it has been  
507 possible to make this interpretation because the Jurassic substrate of both studied sectors is  
508 different; if the Jurassic substrate were carbonate and similar in both sectors, as occurs in many  
509 areas of the Iberian Basin (Gómez, et al. 2004; 2019), it would not have been possible to  
510 accurately evaluate the influence of the riverine water in the  $^{87}\text{Sr}/^{86}\text{Sr}$  of carbonates, considering  
511 that the  $^{87}\text{Sr}/^{86}\text{Sr}$  of Barremian-Aptian marine carbonates, as well as most of those of the  
512 Cretaceous, are in the range of the Jurassic  $^{87}\text{Sr}/^{86}\text{Sr}$  marine values, being even identical for  
513 some periods of time (Jones et al. 1994; McArthur 2001; Prokoph et al. 2008; MacArthur et al.  
514 2012). Thus, our data indicate that caution should be taken when interpreting Sr isotopic data  
515 for performing SIS studies obtained from fossil shells and/or carbonates (even those well-  
516 preserved and/or without direct evidence of detrital input) deposited in coastal and shallow  
517 marine sedimentary environments. This is particularly important for coastal and shallow-marine  
518 carbonates deposited in active tectonic settings. In these settings, the uplifted areas are  
519 significantly prone to weathering and erosion, leading to the common development of alluvial  
520 fan systems that eventually discharge into coastal and shallow marine settings, as occurred in  
521 the Iberian Basin during the Late Jurassic-Early Cretaceous extensional phase.

## 522 **6. Conclusions**

523         The Lower Cretaceous Leza Fm (Camos Basin, N Spain) is an essentially carbonate  
524 unit, which was deposited in the context of the Mesozoic Iberian Extensional System, and  
525 whose deposition and thickness were strongly controlled by faulting of the basin substrate  
526 (mainly composed of Jurassic rocks). A coastal wetland system that included carbonates  
527 deposited in freshwater, marine-influenced, marginal-marine and hypersaline water bodies,  
528 formed at that time in the studied area. This system was laterally related with alluvial fans,  
529 whose deposits (conglomerate, sandstone, sandy limestone and marl), sourced in the faulted  
530 and exposed basin substrate, are interbedded with carbonates.

531         Two sectors have been differentiated, Eastern and Western, based on the sedimentary  
532 features of the Leza Fm deposits and those of the Jurassic substrate, which are slightly  
533 different. In the Eastern Sector, the marine influence is higher with the detrital inputs being  
534 lesser than in the Western Sector; additionally, the Middle and Upper Jurassic rocks of the

535 substrate are essentially siliciclastic in the Eastern Sector but essentially carbonate in the  
536 Western Sector.

537 The  $\delta^{18}\text{O}$  values in both sectors follow the expected trend, in accordance with the  
538 different depositional palaeoenvironments: more negative values (down to  $-7.8\text{‰}$ ) are recorded  
539 in freshwater carbonates and more positive values (up to  $+2.8\text{‰}$ ) in marine to hypersaline  
540 marine facies. However, and independently of the marine or freshwater influence, the  $^{87}\text{Sr}/^{86}\text{Sr}$   
541 ratios of the carbonates in the Western Sector (0.707373-0.707801) are significantly lower and  
542 closer to the published Lower Cretaceous marine  $^{87}\text{Sr}/^{86}\text{Sr}$  ratios, than those obtained in the  
543 Eastern Sector (0.707988-0.709033) although, in this sector, the overall marine influence was  
544 higher and the detrital alluvial input lower.

545 These data strongly support that the  $^{87}\text{Sr}/^{86}\text{Sr}$  ratios of all carbonates studied herein  
546 (freshwater, marine-influenced, marginal-marine, and hypersaline) were strongly controlled by  
547 the Sr ratios of the riverine freshwater, which arrived to the coastal and marine areas after  
548 weathering and eroding the carbonate or siliciclastic rocks of the Jurassic substrate of the basin  
549 that was faulted and exposed, even if there is no petrographic evidence of detrital influence, and  
550 even if the  $\delta^{18}\text{O}$  values of carbonates are coherent with their formation in fresh- to marine and  
551 hypersaline waters.

552 Thus, our data indicate that caution should be taken when interpreting Sr isotopic data  
553 for performing SIS studies obtained from fossil shells and/or carbonates (even those well-  
554 preserved) deposited in coastal and shallow marine sedimentary environments, particularly in  
555 active tectonic settings, such as those occurring in the Iberian Basin during the Late Jurassic  
556 and Early Cretaceous extensional system.

## 557 **Acknowledgements**

558 This work is dedicated to the memory of Dr. Carmen Galindo, who was always ready to  
559 help with a beautiful smile. Thanks to her we have a great Geochronology Laboratory, “right  
560 below our feet”. This research was funded by the Spanish projects PGC2018-094034-B-C21  
561 and CGL2014-52670-P, the ‘Sedimentary geology, palaeoclimate and environmental change’  
562 Research Group of the Complutense University of Madrid–Madrid Community. We are also  
563 grateful to José Manuel Fuenlabrada (Chema), Lora Wingate, Aitor Antón, Juan Carlos

564 Salamanca and Beatriz Moral, for their technical support. Authors thanks Dr. Concha Arenas  
565 and an anonymous reviewer for their constructive suggestions and comments

566

567 **References**

- 568 Allan, J.R. & Matthews, R.K. (1977). Carbon and oxygen isotopes as diagenetic and  
569 stratigraphic tools: data from surface and subsurface of Barbados, West Indies.  
570 *Geology*, 5, 16-20.
- 571 Allan, J.R. & Matthews, R.K. (1982). Isotope signatures associated with early meteoric  
572 diagenesis. *Sedimentology*, 29, 797-817.
- 573 Alonso, A. & Mas, J.R. (1988). El Jurásico Superior marino en el sector Demanda-Cameros (La  
574 Rioja-Soria). *III Coloquio de Estratigrafía y Paleogeografía del Jurásico de España,*  
575 *Logroño, 1988. Programa y resúmenes de comunicaciones*,5-8.
- 576 Alonso, A. & Mas, J.R. (1990). El Jurásico Superior marino en el sector Demanda-Cameros (La  
577 Rioja-Soria). *Cuadernos de Geología Ibérica*, 14, 173-198.
- 578 Alonso, A., & Mas, J.R. (1993). Control tectónico e influencia del eustatismo en la  
579 sedimentación del Cretácico inferior de la Cuenca de Los Cameros. *Cuadernos de*  
580 *Geología Ibérica*, 17, 285-310.
- 581 Anderson, P.S., Wasserbug, G.J. & Inorl, J. (1992). The sources and transport of Sr and Nd  
582 isotopes in the Baltic Sea. *Earth and Planetary Science Letters*, 113, 459-472.
- 583 Arenas, C.; Casanova, J. & Pardo, G. (1997). Stable-isotope characterization of the Miocene  
584 lacustrine systems of Los Monegros (Ebro Basin, Spain): palaeogeographic and  
585 palaeoclimatic implications. *Palaeogeography, Palaeoclimatology, Palaeoecology*, 128,  
586 133-155.
- 587 Arribas, J., Alonso, A., Mas, R., Tortosa, A., Rodas, M., Barrenechea, J.F., Alonso-Azcárate, J.,  
588 & Artigas, R. (2003). Sandstone petrography of continental depositional sequences of a  
589 intraplate rift basin: Western Cameros Basin (North Spain). *Journal of Sedimentary*  
590 *Research*, 73, 309-327.
- 591 Azmy, K., Veizer, J., Wenzel, B., Bassett, M.G. & Copper, P. (1999). Silurian strontium isotope  
592 stratigraphy. *Geological Society of America Bulletin*, 111, 475-483.

- 593 Banner, J.L., Musgrove, M. & Capo, R. (1994). Tracing ground-water evolution in a limestone  
594 aquifer using Sr isotopes: effects of multiple sources of dissolved ions and mineral-  
595 solution reactions. *Geology*, 22, 687-690.
- 596 Banner, J. L. (1995). Application of the trace element and isotope geochemistry of strontium to  
597 studies of carbonate diagenesis. *Sedimentology*, 42, 805–824
- 598 Barbieri, M., Castorina, F., Colalongo, M.L., Pasini, G. & Valani, S.C. (1998). Worldwide  
599 correlation of the Pliocene/Pleistocene GSSP at Vrica (southern Italy) confirmed by  
600 strontium isotope stratigraphy. *Newsletters on Stratigraphy*, 36, 177-187.
- 601 Benito, M.I., & Mas, R. (2002). Evolución diagenética de los carbonatos arrecifales de la  
602 Formación Torrecilla en Cameros y de los carbonatos continentales suprayacentes  
603 (Kimmeridgiense inferior-Titónico) en el sector de Soria. Cuenca de Cameros, N.  
604 España. *Cuadernos de Geología Ibérica*, 28, 65-92.
- 605 Benito, M.I., & Mas, R. (2006). Sedimentary evolution of the Torrecilla Reef Complex in  
606 response to tectonically forced regression (Early Kimmeridgian, Northern Spain).  
607 *Sedimentary Geology*, 183, 31-49.
- 608 Benito, M.I., Lohmann, K.C., & Mas, R. (2001). Discrimination of multiple episodes of meteoric  
609 diagenesis in a Kimmeridgian reefal complex, North Iberian Range, Spain. *Journal of*  
610 *Sedimentary Research*, 71, 280-393.
- 611 Benito, M.I., Lohmann, K.C., & Mas, R. (2005). Late Jurassic paleogeography and paleoclimate  
612 in the Northern Iberian Basin of Spain: constraints from diagenetic records in reefal and  
613 continental carbonates. *Journal of Sedimentary Research*, 75, 82-96.
- 614 Benke, K. (1981). Die Dogger/Malm-Wende in den NW-Keltiberischen Ketten (Spanien) und  
615 angrenzenden Gebieten. *Sedimentologie, Stratigraphie und Paläogeographie. Facies*,  
616 4, 95-164.
- 617 Benke, K.; Dürkoop, A.; Errenst, C. & Mensik, H. (1981). Die Korallenkalke im Ober-Jura der  
618 nordwestlichen Iberischen Ketten (Spanien). *Facies*, 4, 27-94.
- 619 Bodin, S., Fiet, N., Godet, A., Matera, V., Westermann, S., Clément, A., Janssen, N. M. M.,  
620 Stille, P. & Föllmi, K. B. (2009). Early Cretaceous (late Berriasian to early Aptian)

621 palaeoceanographic change along the northwestern Tethyan margin (Vocontian  
622 Trough, southeastern France):  $\delta^{13}\text{C}$ ,  $\delta^{18}\text{O}$  and Sr-isotope belemnite and whole-rock  
623 records. *Cretaceous Research*, 30, 1247–1262.

624 Boix, C., Frijia, G., Vicedo, V., Bernaus, J. M., Di Lucia, M., Parente, M. & Caus, E. (2011).  
625 Larger foraminifera distribution and strontium isotope stratigraphy of the La Cova  
626 limestones (Coniacian–Santonian, “Serra del Montsec”, Pyrenees, NE Spain).  
627 *Cretaceous Research*, 32, 806–822.

628 Bonilla-Rodríguez, A. J., González, L. A., Douglas Walker, J. & Santos, H. (2014). Strontium  
629 isotope ( $^{87}\text{Sr}/^{86}\text{Sr}$ ) stratigraphy from the Coalcomana–Caprinuloidea rudist assemblage  
630 in the Greater Antilles (Puerto Rico, Dominican Republic and Jamaica). *Cretaceous*  
631 *Research*, 50, 97–109.

632 Bover-Arnal, T., Moreno-Bedmar, J.A., Frijia, G., Pascual-Cebrian, E & Salas, R. (2016).  
633 Chronostratigraphy of the Barremian-Early Albiano of the Maestrat Basin (E Iberian  
634 Peninsula): integrating strontium isotope stratigraphy and ammonoid biostratigraphy.  
635 *Newsletters on Stratigraphy*, 49(1), 41-68.

636 Bralower, T.J., Fullagar, P.D., Paull, C.K., Dwyer, G.S. & Leckie, R.M. (1997). Mid-Cretaceous  
637 strontium-isotope stratigraphy of deep-sea sections. *Geological Society of America*  
638 *Bulletin*, 109, 1421-1442.

639 Brasier, M.D., Shields, G.A., Kuleshov, V.N. & Zhegallo, E.A. (1996). Integrated chemo- and  
640 biostratigraphic calibration of early animal evolution: Neoproterozoic-early Cambrian of  
641 southwest Mongolia. *Geological Magazine*, 133, 445-485

642 Brass, G.W. (1976) The variation of the marine  $^{87}\text{Sr}/^{86}\text{Sr}$  ratio during Phanerozoic time:  
643 interpretation using a flux model. *Geochimica et Cosmochimica Acta*, 40, 721-730.

644 Bryant, J.D., Jones, D.S. & Mueller, P.A. (1995). Influence of freshwater flux on  $^{87}\text{Sr}/^{86}\text{Sr}$   
645 chronostratigraphy in marginal marine environments and dating vertebrate and  
646 invertebrate faunas. *Journal of Paleontology*, 69, 1-6.

647 Bulard, P.F. (1972). Le Jurassique Moyen et Supérieur de la Chaîne Ibérique sur la bordure du  
648 bassin de l’Ebre (Espagne). *These Doct. Fac. Sc. Univ. Nice*, 2 vol., 702 pp.



- 649 Burke, W.H., Dension, R.E., Hetherington, E.A., Koepnick, R.B., Nelson, H. & Otto, J.B. (1982).  
650 Variations of seawater  $^{87}\text{Sr}/^{88}\text{Sr}$  throughout Phanerozoic time. *Geology*, 10, 516-519.
- 651 Casas-Sainz, A.M., & Simón-Gómez, J.L. (1992). Stress field and thrust kinematics: a model for  
652 the tectonic inversion of the Cameros Massif (Spain). *Journal of Structural Geology*, 14,  
653 521-530.
- 654 Caus, E., Frijia, G., Parente, M., Robles-Salcedo, R. & Villalonga, R. (2016). Constraining the  
655 age of the last marine sediments in the late Cretaceous of central south Pyrenees (NE  
656 Spain): insights from larger benthic foraminifera and strontium isotope stratigraphy.  
657 *Cretaceous Research*, 57, 402-413.
- 658 DePaolo, D.J. & Ingram, B.L. (1985). High-resolution stratigraphy with strontium isotopes.  
659 *Science*, 227, 938-941.
- 660 Dickson, J.A.D. (1966). Carbonate identification and genesis as revealed by staining. *Journal of*  
661 *Sedimentary Petrology*, 36 (2), 491-505.
- 662 Dunham, R.J. (1962) Classification of carbonate rocks according to depositional texture. In:  
663 Ham, W.E. (Ed.). Classification of Carbonate Rocks. Am. Assoc. Pet. Geol. Memoir, 1,  
664 108–121.
- 665 Durantez, O., Solé, J., Castiella, J. & Villalobos, L. (1982) *Mapa Geológico y Memoria de la*  
666 *Hoja nº 281 (Cervera del Río Alhama). Mapa Geológico de España E. 1:50.000.*  
667 *Segunda Serie (MAGNA)*, ITGE, 41 pp.
- 668 Ebneth, S., Shields, G.A., Veizer, J., Miller, J.F. & Shergold, J.H. (2001). High resolution  
669 strontium isotope stratigraphy across the Cambrian-Ordovician transition. *Geochimica*  
670 *et Cosmochimica Acta*, 65, 2273-2292
- 671 Errenst, C. (1990). Das korallenführende Kimmeridgium der nordwestlichen Iberischen Ketten  
672 und angrenzender gebiete (Fazies, paläogeographie und beschreibung der  
673 korallenfauna). Teil 1. *Palaeontographica*, A, 214 (3-6), 121-207.
- 674 Fan, T., Yu, K., Zhao, J., Jiang, W., Xu, S., Zhang, Y., Wang, R., Wang, Y., Feng, Y., Bian, L.,  
675 Qian, H. & Liao, W. (2020). Strontium isotope stratigraphy and paleomagnetic age

676 constraints on the evolution history of coral reef islands, northern South China Sea. *The*  
677 *Geological Society of America Bulletin*, 132, 803-816.

678 Faure, G. (1977). *Principles of isotope geology*. New York. John Wiley & Sons.

679 Flecker, R., de Villiers, S. & Ellam, R.M. (2002). Modelling the effect of evaporation on the  
680 salinity– $^{87}\text{Sr}/^{86}\text{Sr}$  relationship in modern and ancient marginal-marine systems: the  
681 Mediterranean Messinian. *Earth and Planetary Science Letters*, 203, 221–233.

682 Flecker, R., & Ellam, R. M. (2006). Identifying Late Miocene episodes of connection and  
683 isolation in the Mediterranean–Paratethyan realm using Sr isotopes. *Sedimentary*  
684 *Geology*, 188–189, 189–203.

685 Frank, T.D. & Lohmann, K.C. (1995). Early cementation during marine-meteoric fluid mixing:  
686 Mississippian Lake Valley Formation, New Mexico. *Journal of Sedimentary Research*,  
687 A65, 263-273.

688 Frau, C., Masse, J.P., Fenerci-Masse, M., Tendil, A.J.B., Pictet, A. & Lanteaume, C. (2018). Is  
689 Strontium-isotope stratigraphy a reliable tool for dating shallow-marine platform  
690 carbonates at the Barremian-Aptian transition? Review of western Tethyan case  
691 studies. *Carnets de Geologie*, 18, 139-154.

692 Friedman, I & O’Neil, J.R. (1977). Compilation of stable isotope fractionation factors of  
693 geochemical interest. In: Data of Geochemistry. *U.S. Geological Survey, Professional*  
694 *Paper 440-KK*, p. 1–12.

695 Frijia, G. & Parente, M. (2008). Strontium isotope stratigraphy in the upper Cenomanian  
696 shallow-water carbonates of the southern Apennines: short-term perturbations of marine  
697  $^{87}\text{Sr}/^{86}\text{Sr}$  during the oceanic anoxic event 2. *Palaeogeography, Palaeoclimatology,*  
698 *Palaeoecology*, 261, 15–29.

699 Frijia, G., Parente, M., Di Lucia, M. & Mutti, M. (2015). Carbon and strontium isotope  
700 stratigraphy of the Upper Cretaceous (Cenomanian–Campanian) shallow-water  
701 carbonates of southern Italy: Chronostratigraphic calibration of larger foraminifera  
702 biostratigraphy. *Cretaceous Research*, 53, 110–139.

- 703 Fritz, P. & Smith, D.G.W. (1970). The isotopic composition of secondary dolomites. *Geochimica*  
704 *et Cosmochimica Acta*, 34, 1161-1173.
- 705 García-Frank, A., Ureta, S. & Mas, R. (2008). Aalenian pulses of tectonic activity in the Iberian  
706 Basin, Spain. *Sedimentary Geology*, 209, 15–35.
- 707 Gierlowski-Kordesch, E.H. & Cassle, C.F. (2015). The “Spirorbis” problem revisited:  
708 Sedimentology and biology of microconchids in marine-nonmarine transitions. *Earth*  
709 *Science Reviews*, 148, 209-227.
- 710 Gómez Fernández, J.C. (1992). *Análisis de la Cuenca sedimentaria de los Cameros durante*  
711 *sus etapas iniciales de relleno en relación con su evolución paleogeográfica*. Tesis  
712 Doctoral, Univ. Complutense de Madrid, 343 pp. Unpublished
- 713 Gómez, J.J., Fernández-López, S. & Goy, A. (2004). 5.3.2. Primera fase de postrifting: Jurásico  
714 Inferior y Medio. In: J.A. Vera (Ed.). *Geología de España* (pp. 495-503). Madrid. SGE-  
715 IGME.
- 716 Gómez, J.J., Aguado, R., Azeredo, A.C., Cortés, J. E., Duarte, L.V., O’Dogherty, L., Bordalo da  
717 Rocha & Sandoval, J. (2019). The Late Triassic-Middle Jurassic Passive Margin Stage.  
718 In: C. Quesada & J.T. Oliveira (Eds.), *The geology of Iberia: A geodynamic approach*  
719 (pp. 113-168). Switzerland. Springer.
- 720 Guimerà, J., Alonso, A. & Mas, J. R. (1995). Inversion of an extensional-ramp basin by a newly  
721 formed thrust: the Cameros Basin (N. Spain). In: J. G. Buchanan, and P. G. Buchanan  
722 (Eds.), *Basin Inversion. Geological Society Special Publications*, 88, 433-453.
- 723 Guiraud, M. (1983). *Evolution tectono-sédimentaire du bassin Wealdien (Crétacé inférieur) en*  
724 *relais de décrochements de Logroño-Soria (NW Espagne)*. Tesis Doctoral. Univ.  
725 Sciences et Techniques du Languedoc, 183 pp. Unpublished.
- 726 Guiraud, M. & Séguret, M. (1985). A releasing solitary overstep model for the late Jurassic-early  
727 Cretaceous (Wealdian) Soria strike-slip Basin (northern Spain). *SEPM, Spec. Public.*,  
728 37, 159-175.
- 729 Hernández-Samaniego, A., Ramirez Merino, J.I., Olivé Davó, A., Alvaro López, M., Ramírez del  
730 Pozo, J., Aguilar, M.J. & Meléndez Hevia, A. (1990). *Mapa Geológico y Memoria de la*

- 731            *Hoja nº 242 (Munilla). Mapa Geológico de España E. 1:50.000. Segunda Serie*  
732            *(MAGNA)*, ITGE, 55 pp.
- 733    Hess, J., Scott, L.D., Bender, M.L., Kennet, J.P. & Schiling, J.G. (1989). The Oligocene marine  
734            microfossil record: age assessments using strontium isotopes. *Paleoceanography*, 4,  
735            655-679.
- 736    Hofer, G., Wagreich, M & Spotl, C. (2013). Carbon, oxygen and strontium isotopes as a tool to  
737            decipher marine and non-marine environments: Implications from a case study of cyclic  
738            Upper Cretaceous sediments. In: A.V. Bojar, M.C. Melinte-Dobrinescu & J. Smith (Eds.)  
739            *Isotopic studies in Cretaceous research. Geological society Special Publication*, 382,  
740            123-141.
- 741    Hudson, J.D. (1977). Stable isotopes and limestone lithification. *Journal of the Geological*  
742            *Society of London*, 133, 637-660
- 743    Ingram, B.L. & Sloan, D. (1992). Strontium isotopic composition of estuarine sediments as  
744            paleosalinity-paleoclimate indicator. *Science*, 255, 68-72.
- 745    James, N.P. & Choquette, P.W. (1990). Limestones-The meteoric diagenetic environment. In:  
746            I.A. McIlreath, D.W. Morrow (Eds.), *Diagenesis*, *Geoscience Canada, Reprint Series*, 4,  
747            35-73.
- 748    Jenkyns, H.C., Jones, C.E., Gröcke, D.R., Hesselbo, S.P. & Parkinson, D.N. (2002).  
749            Chemostratigraphy of the Jurassic System: applications, limitations and implications for  
750            palaeoceanography. *Journal of the Geological Society of London*, 159, 351–378.
- 751    Jones, C.E., Jenkyns, H.C.; Coe, A.L. & Hesselbo, S.P. (1994). Sr-isotopic variations in Jurassic  
752            and Cretaceous seawater. *Geochimica et Cosmochimica Acta*, 58, 3061–3074.
- 753    Koepnick, R.B., Denison, R.E. & Dahl, D.A. (1988). The Cenozoic sea water <sup>87</sup>Sr/<sup>86</sup>Sr curve:  
754            data review and implications for correlation of marine strata. *Paleoceanography*, 3, 743-  
755            756.
- 756    Korte, C. & Ullmann (2016). Permian strontium isotope stratigraphy. In: S.G. Lucas & S.Z. Shen  
757            (Eds) *The Permian Timescale. Geological Society, London, Special Publications*, 450,  
758            1-12.

- 759 Leng, M.J. & Marshall, J.D. (2004) Palaeoclimate interpretation of stable isotope data from lake  
760 sediments archives. *Quaternary Science Reviews*, 23, 7-8.
- 761 Lohmann, K.C. (1987). Geochemical patterns of meteoric diagenetic systems and their  
762 application to studies of paleokarst. In: N.P. James, P.W. Choquette (Eds), *Paleokarst*  
763 (pp. 58-80). New York. *Springer-Verlag*,.
- 764 Lugli, S., Manzi, V., Roveri, M., & Schreiber, B. C. (2010). The Primary Lower Gypsum in the  
765 Mediterranean: a new facies interpretation for the first stage of the Messinian salinity  
766 crisis. *Palaeogeography, Palaeoclimatology, Palaeoecology*, 297, 83–99.
- 767 Madhavaraju, J., Scott, R.W., Selvaraj, K., Lee, Y.I.L. & Löser, H. (2020). Isotopic  
768 chemostratigraphy and biostratigraphy of Lower Cretaceous Alisitos Formation (Punta  
769 China section), Baja California, Mexico. *Geological Journal*, 1-21.
- 770 Manzi, V., Gennari, R., Lugli, S., Persico, D., Reghizzi, M., Roveri, M. & Gvirtzman, Z. (2018).  
771 The onset of the Messinian Salinity Crisis in the deep Eastern Mediterranean Basin.  
772 *Terra Nova*, 30, 189–198
- 773 Martín-Chivelet, J., López-Gómez, J., Aguado, R., Arias, C., Arribas, J., Arribas, M.E., Aurell,  
774 M., Bádenas, B., Benito, M.I., Bover-Arnal, T., Casas-Sainz, A., Castro, J.M., Coruña,  
775 F., de Gea, G.A., Fornós, J.J., Fregenal-Martínez, M., García-Senz, J., Garófano, D.,  
776 Gelabert, B., Giménez, J., González-Acebrón, L., Guimerà, J., Liesa, C., Mas, R.,  
777 Meléndez, N., Molina, J.M., Muñoz, J.A., Navarrete, R., Nebot, M., Nieto, L.M.,  
778 Omodeo-Salé, S., Pedrera, A., Peropadre, C., Quijada, I.E., Quijano, M.L., Reolid, M.,  
779 Robador, A., Rodríguez-López, J.P., Rodríguez-Perea, A., Rosales, I., Ruiz-Ortiz, P.A.,  
780 Sàbat, F., Salas, R., Soria, A.R., Suarez-Gonzalez, P., Vilas, L. (2019). The Late  
781 Jurassic-Early Cretaceous Rifting. In: Quesada, C., Oliveira, J.T. (Eds.), *The Geology of*  
782 *Iberia: A Geodynamic Approach* (pp. 169-249). Switzerland. Springer.
- 783 Mas, R., Alonso, A., & Guimerà, J. (1993) Evolución Tectonosedimentaria de una Cuenca  
784 Extensional Intraplaca: La Cuenca Finijurásica-Eocretácica de Los Cameros (La Rioja-  
785 Soria). *Revista de la Sociedad Geológica de España*, 6, 129–144.
- 786 Mas, R., M. I. Benito, J. Arribas, A. Serrano, J. Guimerà, A. Alonso, & J. Alonso-Azcárate,  
787 2002a. La Cuenca de Cameros: desde la extensión finijurásica-eocretácica a la

788 inversión Terciaria - Implicaciones en la exploración de hidrocarburos, *Zubía*  
789 *Monográfico*, 14, 9-64.

790 Mas, J.R., Benito, M.I., Arribas, J., Alonso, A., Arribas, M.E., Lohmann, K.C, Hernán, J.,  
791 Quijada, E., Suárez, P., & Omodeo-Salé, S. 2011. Evolution of an intra-plate rift basin:  
792 the Latest Jurassic–Early Cretaceous Cameros Basin (Northwest Iberian Ranges, North  
793 Spain). In L. Pomar, & C. Arenas (Eds.), *Geo-Guías*, 8. *Post-Meeting field trips*, 28th  
794 *International Association of Sedimentologists*, Zaragoza (pp. 117–154).

795 Mas, R., Arribas, M.E., González-Acebrón, L., Quijada, I.E., Campos-Soto, S., Suarez-  
796 Gonzalez, P., Sacristán-Horcajada, S., Arribas, J., Benito, M.I., Pérez-Garrido, C.,  
797 Alonso, A. (2019). Coastal wetlands as markers of transgression in proximal extensional  
798 systems (Berriasian, W Cameros Basin, Spain). *Journal of Iberian Geology*, 45, 1–27.

799 Mase, J.P., Bouaziz, S., Amon, E.O., Trakowski, R., Sandulescu, M., Platel, J.P., Canerot, J.,  
800 Guiraud, R., Poisson, A., Ziegler, M., Rimmelé, G. and collaborators (2000). Early  
801 Aptian. In J. Decorut, M. Gaetani, B. Vrielynck, E. Barrier, B. Biju-Duval, M. F. Brunet, J.  
802 P. Cadet, S. Crasquin, M. Sandulescu (Eds.), *Atlas peri-Tethys palaeogeographical*  
803 *maps (Map-13)*. Paris: CCGM.

804 McArthur, J. M. (1994). Recent trends in strontium isotope stratigraphy. *Terra Nova*, 6, 331–  
805 358.

806 McArthur, J.M., Burnett, J. & Hancock, J.M. (1992). Strontium isotope stratigraphy in the Late  
807 Cretaceous intercontinental correlation of the Campanian/Maastrichtian boundary. *Terra*  
808 *Nova*, 4, 385-393.

809 McArthur, J.M., Chen, M., Gale, A.S., Thirlwall, M.F. & Kennedy, W.J. (1993). Strontium isotope  
810 stratigraphy for the Late Cretaceous: Age models and intercontinental correlations for  
811 the Campanian. *Paleoceanography*, 8, 859-873.

812 McArthur, J.M., Kennedy, W.J., Chen, M., Thirlwall, M.F. & Gale, A.S. (1994). Strontium isotope  
813 stratigraphy for the Late Cretaceous: Direct numerical age calibration of the Sr-isotope  
814 curve for the U.S. Western Interior Seaway. *Palaeogeography, Palaeoclimatology,*  
815 *Palaeoecology*, 108, 95-119.

- 816 McArthur, J.M., Donovan, D.T., Thirlwall, M.F., Fouke, B.W. & Matthey, D. (2000). Strontium  
817 isotope profile of the Early Toarcian (Jurassic) Oceanic Anoxic Event, the duration of  
818 ammonite biozones, and belemnite palaeotemperatures. *Earth and Planetary Science*  
819 *Letters*, 179, 269-285.
- 820 McArthur, J. M., Howarth, R. J., & Bailey, T. R. (2001). Strontium isotope stratigraphy: LOWESS  
821 version 3: Best fit to the marine Sr-isotope curve for 0-509 Ma and accompanying  
822 look-up table for deriving numerical age. *The Journal of Geology*, 109, 155–170.
- 823 McArthur, J.M., Janssen, N.M.M., Reboulet, S., Leng, M.J., Thirlwall, M.F. & van de  
824 Schootbrugge, B. (2007). Early Cretaceous ice-cap volume, palaeo-temperatures (Mg,  
825  $\delta^{18}\text{O}$ ), and isotope stratigraphy ( $\delta^{13}\text{C}$ ,  $^{87}\text{Sr}/^{86}\text{Sr}$ ) from Tethyan belemnites.  
826 *Palaeogeography, Palaeoclimatology, Palaeoecology*, 248, 391-430.
- 827 McArthur, J.M., Howarth, R. J., & Shields, G. A. (2012). Strontium isotope stratigraphy. In: F. M.  
828 Gradstein, J. G. Ogg, M. D. Schmitz, & G. M. Ogg (Eds.), *The Geological Time Scale*  
829 2012 (pp. 127–144). Oxford: Elsevier B.V.
- 830 McKenzie, J.A. (1981). Holocene dolomitization of calcium carbonate sediments from the  
831 coastal sabkhas of Abu Dhabi, UAE: a stable isotope study. *The Journal of Geology*, 89,  
832 185-198.
- 833 Meknassi, S.; Dera, G.; Cardone, T.; De Rafélis, M.; Brahmi, C. & Chavagnac, V. (2018). Sr  
834 isotope ratios of modern carbonate shells: Good and bad news for chemostratigraphy.  
835 *Geology*, 1003-1006.
- 836 Mensink, H. (1966). Stratigraphie und Paläogeographie des marinen Jura in den nordwestlichen  
837 Iberischen Ketten (Spanien). *Beihefte zum Geologischen Jahrbuch*, 44, 55-102.
- 838 Miller, K.G., Feigenson, M.D., Kent, D.V. & Olson, R.K. (1988). Upper Eocene to Oligocene  
839 isotope ( $^{87}\text{Sr}/^{86}\text{Sr}$ ,  $\delta^{18}\text{O}$ ,  $\delta^{13}\text{C}$ ) standard section, *Deep Sea Drilling Project Site 522*.  
840 *Paleoceanography*, 3, 223-233.
- 841 Müller, D.W. & Mueller, P.A. (1991). Origin and age of the Mediterranean Messinian evaporites:  
842 implications from Sr isotopes. *Earth and Planetary Science Letters*, 107, 1–12.

- 843 Müller, D.W., McKenzie, J.A. & Mueller, P.A. (1990). Abu Dhabi sabkha, Persian Gulf, revisited:  
844 application of strontium isotopes to test an early dolomitization model. *Geology*, 18,  
845 618-621.
- 846 Nieto, L.M., Ruiz-Ortiz, P.A., Rey, J. & Benito, M.I. (2008). Sr-Isotope Stratigraphy (SIS)  
847 elucidates the age of condensed levels: Examples from the Subbetic (Southern Spain).  
848 *Sedimentology*, 55, 1–29.
- 849 Ochoa, M. (2006). *Procedencia y diagénesis del registro arenoso del Grupo Urbión (Cretácico*  
850 *inferior) de la Cuenca de Cameros (Cordillera Ibérica septentrional)*. Unpublished PhD  
851 Thesis. Universidad Complutense de Madrid.
- 852 Omodeo-Salé, S., Guimerà, J., Mas, R., & Arribas, J. 2014. Tecono-Stratigraphic Evolution of  
853 an Inverted Extensional Basin: The Cameros Basin (North of Spain). *International*  
854 *Journal of Earth Sciences*, 103, (6), 1597-1620.
- 855 Omodeo-Salé, S., Salas, R., Guimerà, J., Ondrak, R., Suarez-Ruiz, I., Martinez, L., Mas, R., &  
856 Arribas, J. (2015). Subsidence and thermal history of an inverted Late Jurassic-Early  
857 Cretaceous extensional basin (Cameros, North-central Spain) affected by very low- to  
858 low-grade metamorphism. *Basin Research*, 1-19.
- 859 Platt, N. H. (1990). Basin evolution and fault reactivation in the western Cameros basin,  
860 Northern Spain. *Journal of the Geological Society*, London, 147: 165-175.
- 861 Price, G.D. & Gröcke, D.R. (2002) Strontium-isotope stratigraphy and oxygen- and carbon-  
862 isotope variation during the Middle Jurassic-Early Cretaceous of the Falkland Plateau,  
863 South Atlantic. *Palaeogeography Palaeoclimatology Palaeoecology*, 183, 209–222.
- 864 Prokoph, A., Shields, G.A. & Veizer, J. (2008). Compilation and time-series analysis of a marine  
865 carbonate  $\delta^{18}\text{O}$ ,  $\delta^{13}\text{C}$ ,  $^{87}\text{Sr}/^{86}\text{Sr}$  and  $\delta^{34}\text{S}$  database through Earth history. *Earth Science*  
866 *Reviews*, 87, 113–133.
- 867 Quijada, I.E, Suarez-Gonzalez, P., Benito, M.I. & Mas, R. (2013a). New insights on stratigraphy  
868 and sedimentology of the Oncala Group (eastern Cameros Basin): implications for the  
869 paleogeographic reconstruction of NE Iberia at Berriasian times: *Journal of Iberian*  
870 *Geology*, 39, 313–334.



871 Quijada, I.E., Suarez-Gonzalez, P., Benito, M.I., & Mas, R. (2013b). Depositional depth of  
872 laminated carbonate deposits: insights from the Lower Cretaceous Valdeprado  
873 Formation (Camereros Basin, northern Spain). *Journal of Sedimentary Research*, 83,  
874 241-257.

875 Quijada, I.E., Suarez-Gonzalez, P., Benito, M.I., Lugli, S., & Mas, R. (2014). From carbonate-  
876 sulphate interbeds to carbonate breccias: The role of tectonic deformation and  
877 diagenetic processes (Camereros Basin, Lower Cretaceous, N Spain). *Sedimentary  
878 Geology*, 312, 76-98.

879 Quijada, I.E., Suarez-Gonzalez, P., Benito, M.I. & Mas, R. (2016a). Los isótopos de S en los  
880 yesos del Grupo Oncala: evidencia de influencia marina en los depósitos carbonáticos-  
881 evaporíticos berriasienses de la cuenca de Cameros (La Rioja-Sonia). *Geo-Temas* 16,  
882 555-558.

883 Quijada, I.E, Suarez-Gonzalez, P., Benito, M.I., & Mas, R. 2016b: Tidal *versus* continental  
884 sandy\_muddy flat deposits: Evidence\_from\_the Oncala Group (Early Cretaceous, N  
885 Spain). In B. Tessier and J.Y. Reynaud (Eds.), *Contributions to Modern and Ancient  
886 Tidal Sedimentology: Proceedings of the Tidalites 2012 Conference* (pp. 133-159).  
887 International Association of Sedimentologists. John Wiley & Sons, Ltd.

888 Quijada, I.E., Benito, M.I.; Suarez-Gonzalez, P., Rodríguez-Martínez, M. & Campos-Soto, S.  
889 (2020). Challenges to carbonate-evaporite peritidal facies models and cycles: insights  
890 from Lower Cretaceous stromatolite-bearing deposits (Oncala Group, N Spain).  
891 *Sedimentary Geology*. In press. <https://doi.org/10.1016/j.sedgeo.2020.105752>

892 Ramírez-Merino, J.I., Olivé Davó, A., Hernández Samaniego, A., Alvaro López, M., Aguilar,  
893 M.J., Ramirez del Pozo, J., Anadón, P., Molina, E., Gallardo, J. (1990). *Mapa Geológico  
894 y Memoria de la Hoja nº 241 (Anguiano)*. *Mapa Geológico de España E. 1:50.000.  
895 Segunda Serie (MAGNA)*, ITGE, 63 pp.

896 Rat, J., Mouthereau, F., Brichau, S., Crémades, A., Bernet, M., Balvay, M., Ganne, J., Lahfid, A.  
897 & Gautheron, C. (2019). Tectonothermal evolution of the Cameros basin: Implications  
898 for tectonics of North Iberia. *Tectonics*, 38, 440-469.

- 899 Reghizzi, M., Gennari, R., Douville, E., Lugli, S., Manzi, V., Montagna, P. & Taviani, M. (2017).  
900 Isotope stratigraphy ( $^{87}\text{Sr}/^{86}\text{Sr}$ ,  $\delta^{18}\text{O}$ ,  $\delta^{13}\text{C}$ ) of the Sorbas basin (Betic Cordillera, Spain):  
901 Paleooceanographic evolution across the onset of the Messinian salinity crisis.  
902 *Palaeogeography, Palaeoclimatology, Palaeoecology*, 469, 60–73.
- 903 Roveri, M., Lugli, S., Manzi, V., Gennari, R., & Schreiber, B. C. (2014). High-resolution strontium  
904 isotope stratigraphy of the Messinian deep Mediterranean basins: Implications for  
905 marginal to central basins correlation. *Marine Geology*, 349, 113–125.
- 906 Roveri, M., Gennari, R., Persico, D., Rossi, F.P., Lugli, S., Manzi, V., Reghizzi, M. & Taviani, M.  
907 (2019). A new chronostratigraphic and palaeoenvironmental framework for the end of  
908 the Messinian salinity crisis in the Sorbas Basin (Betic Cordillera, southern Spain).  
909 *Geological Journal*, 54, 1617-1637.
- 910 Sacristán-Horcajada, S., Mas, R., & Arribas, M.E. 2015. Early syn-rift evolution in the W  
911 Cameros Basin (Upper Jurassic, NW Iberian Range) Spain. *Journal of Sedimentary*  
912 *Research*, 85, 794–819.
- 913 Sacristán-Horcajada, S., Arribas, M.E., & Mas, R. 2016. Pedogenetic calcretes in early syn-rift  
914 alluvial systems (Upper Jurassic, West Cameros Basin), northern Spain. *Journal of*  
915 *Sedimentary Research*, 86, 268-286.
- 916 Salas, R. & Casas, A. (1993). Mesozoic extensional tectonics, stratigraphy and crustal evolution  
917 during the Alpine cycle of the eastern Iberian basin. *Tectonophysics*, 228(1-2), 33–55.  
918 [https://doi.org/10.1016/0040-1951\(93\)90213-4](https://doi.org/10.1016/0040-1951(93)90213-4)
- 919 Salas, R., Guimerà, J., Mas, R., Martín-Closas, C., Melendez, A. & Alonso, Á. (2001). Evolution  
920 of the Mesozoic central Iberian rift system and its Cainozoic inversion (Iberian chain).  
921 *Memoires Du Museum National d'Histoire Naturelle*, 186, 145–186.
- 922 Scasso, R.A., McArthur, J.M., del Río, C.J., Martínez, S.A. & Thirlwall, M.F. (2001).  $^{87}\text{Sr}/^{86}\text{Sr}$   
923 late Miocene age of fossil molluscs in the “entrerriense” of Valdés península (Chubut,  
924 Argentina). *Journal of South American Earth Sciences*, 14, 319–329.

- 925 Schmitz, B., Åberg, G., Werdelin, L., Forey, P. & Bendix-Almgreen, S. (1991).  $^{87}\text{Sr}/^{86}\text{Sr}$ , Na, F,  
926 Sr, and La in skeletal fish debris as a measure of the paleosalinity of fossil-fish habitats.  
927 *Geological Society of America Bulletin*, 103, 786-794.
- 928 Sessa, J.A., Ivany, L.C., Schlossnagle, T.H., Samson, S.D. & Schellenberg, S.A. (2012). The  
929 fidelity of oxygen and strontium isotope values from shallow shelf settings: Implications  
930 for temperature and age reconstructions. *Palaeogeography, Palaeoclimatology,*  
931 *Palaeoecology*, 342-343, 27-39.
- 932 Steuber, T. (2001). Strontium isotope stratigraphy of Turonian-Campanian Gosau-type rudist  
933 formations in the Northern Calcareous and Central Alps (Austria and Germany).  
934 *Cretaceous Research*, 22, 429–441.
- 935 Steuber, T. & Veizer, J. (2002). Phanerozoic record of plate tectonic control of seawater  
936 chemistry and carbonate sedimentation. *Geology*, 30, 1123–1126.
- 937 Steuber, T. & Schlüter, M. (2012). Strontium-isotope stratigraphy of Upper Cretaceous rudist  
938 bivalves: biozones, evolutionary patterns and sea-level change calibrated to numerical  
939 ages. *Earth-Science Reviews*, 114, 42–60.
- 940 Stueber, A.M., Pushkar, P. & Hetherington, E.A. (1984). A strontium isotopic study of  
941 Smackover brines and associated solids, southern Arkansas. *Geochimica et*  
942 *Cosmochimica Acta*, 48, 1637-1649.
- 943 Stueber, A.M., Pushkar, P. & Hetherington, E.A. (1987). A strontium isotopic study of formation  
944 waters from the Illinois Basin, U.S.A. *Applied Geochemistry*, 2, 477-494.
- 945 Suarez-Gonzalez, P (2015). *Sedimentología y paleogeografía de los sistemas de humedales*  
946 *costeros de la Fm Leza (Cretácico Inferior, Cuenca de Cameros): implicaciones en el*  
947 *origen y desarrollo de los depósitos microbianos asociados*. Ph. D. Thesis, Universidad  
948 Complutense de Madrid. 363 pp. ISBN: 978-84-608-3251-5
- 949 Suarez-Gonzalez, P., Quijada, I.E., Benito, M.I., & Mas, R. 2013. Eustatic versus tectonic  
950 control in an intraplate rift basin (Leza Fm, Cameros Basin): chronostratigraphic and  
951 paleogeographic implications for the Aptian of Iberia: *Journal of Iberian Geology*, 39,  
952 285–312.

- 953 Suarez-Gonzalez, P., Quijada, I.E., Benito, M.I., Mas, R., Merinero, R. & Riding, R. (2014).  
954 Origin and significance of lamination in Lower Cretaceous stromatolites and proposal for  
955 a quantitative approach. *Sedimentary Geology*, 300, 11-27.
- 956 Suarez-Gonzalez, P., Quijada, I.E., Benito, M.I., & Mas, R. 2015. Sedimentology of ancient  
957 coastal wetlands: Insights from a Cretaceous multifaceted depositional system. *Journal*  
958 *of Sedimentary Research*, 85, 95-117.
- 959 Suarez-Gonzalez, P., Benito, M.I., Mas, R., Quijada, I.E., & Campos-Soto, S. (2016a).  
960 Influencia del Keuper y de la estructuración tardivarisca en la arquitectura de las  
961 unidades sin-extensionales del borde norte de la Cuenca de Cameros. *Geo-Temas*, 15,  
962 185-188.
- 963 Suarez-Gonzalez, P., Quijada, I.E., Benito, M.I., Mas, R. (2016b). Do stromatolites need tides to  
964 trap ooids? Insights from a Cretaceous system of coastal-wetlands. In: B. Tessier & J.Y.  
965 Reynaud (Eds.) *Contributions to Modern and Ancient Tidal Sedimentology: Proceedings*  
966 *of the Tidalites 2012 Conference* (pp. 161-190. International Association of  
967 Sedimentologists. John Wiley & Sons, Ltd.
- 968 Suarez-Gonzalez, P., Benito, M.I., Quijada, I.E., Mas, R., Campos-Soto, S. (2019). 'Trapping  
969 and binding': A review of the factors controlling the development of fossil agglutinated  
970 microbialites and their distribution in space and time. *Earth-Science Reviews*, 194, 182-  
971 215.
- 972 Topper, R.P.M. & Meijer, P.Th. (2013). A modelling perspective on spatial and temporal  
973 variations in Messinian evaporite deposits. *Marine Geology*, 336, 44–60.
- 974 Topper, R.P.M., Flecker, R., Meijer, P.Th. & Wortel, M.J.R. (2011). A box model of the Late  
975 Miocene Mediterranean Sea: implications from combined  $^{87}\text{Sr}/^{86}\text{Sr}$  and salinity data.  
976 *Paleoceanography*, 26, PA3223
- 977 Tucker, M. & Wright, V.P. (1990). *Carbonate sedimentology*. Blackwell scientific publications.  
978 Oxford.
- 979 Veizer, J. & Compston, W. (1974).  $^{87}\text{Sr}/^{86}\text{Sr}$  composition of seawater during the Phanerozoic.  
980 *Geochimica et Cosmochimica Acta*, 38, 1461–1484.

981 Veizer, J., Buhl, D., Diener, A., Ebner, S., Podlaha, O.G., Bruckschen, P., Jasper, T., Korte, C.,  
982 Schaaf, M., Ala, D. & Azmy, K.; (1997). Strontium isotope stratigraphy: potential  
983 resolution and event correlation. *Palaeogeography, Palaeoclimatology, Palaeoecology*,  
984 132, 65-77.

985 Veizer, J., Ala, D., Azmy, K.; Bruckschen, P., Buhl, D., Bruhn, F., Carden, G.A.F., Diener, A.,  
986 Ebner, S., Godderis, Y., Jasper, T.; Korte, C.; Pawelleck, F., Podlaha, O.G. & Strauss,  
987 H. (1999).  $^{87}\text{Sr}/^{86}\text{Sr}$ ,  $\delta^{13}\text{C}$  and  $\delta^{18}\text{O}$  evolution of Phanerozoic seawater. *Chemical*  
988 *Geology*, 161, 59–88.

989 Warren, J.K., (2016). *Evaporites: A geological compendium*. Heidelberg. Springer,

990 Weedon, G.P. & Jenkyns, H.C. (1999). Cyclostratigraphy and the Early Jurassic timescale: Data  
991 from the Belemnite Marls, southern England. *Geological Society of America Bulletin*,  
992 111, 1823-1840.

993 Wehmiller, J.F., Burleigh Harris, W., Boutin, B.S. & Farrell, K.M. (2012). Calibration of amino  
994 acid racemization (AAR) kinetics in United States mid-Atlantic Coastal Plain Quaternary  
995 mollusks using  $^{87}\text{Sr}/^{86}\text{Sr}$  analyses: Evaluation of kinetic models and estimation of  
996 regional Late Pleistocene temperature history. *Quaternary Geochronology*, 7, 21-36.

997 Wierzbowski, H., Anckiewicz, R., Pawlak, J. & Rogov, M.A. (2017). Revised Middle-Upper  
998 Jurassic strontium isotope stratigraphy. *Chemical Geology*, 466, 239-255.

999 Wilde, S. (1990). The Bathonian and Callovian of the Northwest-Iberian Range: Stages of facial  
1000 and paleogeographical differentiation on an epicontinental platform. *Cuadernos de*  
1001 *Geología Ibérica*, 14, 113-142.

1002 Williamson, T., Henderson, R. A., Price, G. D. & Collerson, K. D. (2012). Strontium-isotope  
1003 stratigraphy of the Lower Cretaceous of Australia. *Cretaceous Research*, 36, 24–36.

1004 Zuo, F., Heinhofer, U., Huck, S., Bodin, S., Erbacher, J. & Bai, H. (2018). Coupled  $\delta^{13}\text{C}$  and  
1005  $^{87}\text{Sr}/^{86}\text{Sr}$  chemostratigraphy of Kimmeridgian shoal-water deposits: A new composite  
1006 record from the Lower Saxony Basin, Germany. *Sedimentary Geology*, 376, 18-31.

1007

1008 **Figure captions**

1009 **Fig. 1.** Geological setting of the studied area. **A.** Map of the Iberian Peninsula, showing the pre-  
1010 Mesozoic Variscan Massif and the Mesozoic Iberian Extensional System (MIES). Red square  
1011 marks the location of the Cameros Basin. **B.** Geological map of the Cameros Basin showing the  
1012 location of the studied area. Red square marks the location of Figs. 2A and 3. **C.** Chrono- and  
1013 lithostratigraphic chart of the eight depositional sequences (DS) of the Cameros Basin  
1014 sedimentary infill, modified after Mas et al. (2011). The Leza Fm (highlighted in red) is part of  
1015 DS7, Late Barremian – Early Aptian in age.

1016 **Fig. 2. A.** Detailed geological map of the northernmost margin of the Cameros Basin (modified  
1017 from Suarez-Gonzalez et al. 2015). Note the tectonic control and individualization of outcrops of  
1018 the Jubera and Leza Fms, deposited mostly on top of the Bathonian to Kimmeridgian marine  
1019 Jurassic substrate of the basin and, locally, over the pre-Bathonian marine Jurassic or over the  
1020 Triassic Keuper facies. Note that the Jubera plus Leza Fms lithotopes are limited by faults, and  
1021 that the colour code of this map is equivalent to that of the stratigraphic chart of Fig. 1C. **B.**  
1022 Correlation panel of the stratigraphic sections showing the thickness of the Jubera and Leza  
1023 Fms (the stratigraphic sections analysed in this study, the Leza River section (LZ), in the  
1024 Western Sector, and the Prójano section (PR), in the Eastern Sector, are highlighted with red  
1025 asterisks). On top, to the right, there is a simplified map showing the location of each section  
1026 and the correlation line (in blue). The top of the Leza Fm has been used as datum for  
1027 correlation. The thickness of the Jubera Fm has been obtained from Ochoa (2006), Hernández-  
1028 Samaniego et al. (1990) and our own measurements. Note the tectonic control of the Jubera  
1029 and Leza Fms and the lateral facies change between the Jubera and Leza Fms. Modified from  
1030 Suarez-Gonzalez et al. 2013.

1031 **Fig. 3. A.** Palaeogeographic map of NE Iberian Peninsula during deposition of the Leza Fm.  
1032 (modified from Suarez-Gonzalez et al. 2013) **B.** Detailed palaeogeographical scheme showing a  
1033 general interpretation of the spatial distribution of depositional environments in NE Cameros  
1034 Basin during sedimentation of the Leza Fm coastal wetlands and the complex array of  
1035 sedimentary environments that characterizes these multifaceted depositional systems (see  
1036 location in A; modified from Suarez-Gonzalez et al., 2015). The map covers approximately the  
1037 same area as the map in Fig. 2A (see names of the main towns in both maps). White areas

1038 represent zones with no outcrops of Lower Cretaceous rocks. These areas may have been  
1039 those where the Jurassic substrate of the Cameros Basin cropped out during sedimentation,  
1040 being the source of the Leza Fm alluvial sediments.

1041 **Fig. 4. A.** Field photograph showing conglomerates of the Leza Fm at the Western Sector,  
1042 where they are mainly composed of fragments of Jurassic carbonates. **B.** Transmitted light  
1043 photomicrograph showing in detail the detrital facies of the Leza Fm at the Western Sector.  
1044 Note that many clasts are composed of oolitic limestone (JL) and reworked single ooids (JO)  
1045 and echinoderms fragments (blue arrow), which are identical to those of the Upper Jurassic  
1046 limestone deposited in the studied area, and other carbonate extraclasts (red arrows) of  
1047 unknown origin. Quartz grains (Q), are also present in variable amounts. **C-D.** Field  
1048 photographs of the detrital alluvial sediments of the Leza Fm at the Eastern Sector. **C.** Very  
1049 poorly sorted conglomerate made up of large marine sandstone clasts (yellow arrows), quartzite  
1050 pebbles (white), and sandy matrix. Coin is 2.3 cm in diameter. **D.** Poorly-sorted conglomerate  
1051 made up mainly of quartzite pebbles (white) in a carbonate matrix.

1052 **Fig. 5.** Detailed stratigraphic sections used for isotopic analyses: the Leza River section, in the  
1053 Western Sector, and the Préjano section, in the Eastern Sector (see Fig. 2 for location). In each  
1054 section the  $\delta^{18}\text{O}$  (pink) and the  $^{87}\text{Sr}/^{86}\text{Sr}$  (black) are shown. The range of published  $\delta^{18}\text{O}$  and  
1055  $^{87}\text{Sr}/^{86}\text{Sr}$  values for the Barremian-Aptian marine carbonates and, in the case of the Sr isotopes,  
1056 for the Jurassic are also shown. Blue circles represent the depositional environment where the  
1057 different carbonate facies were deposited.

1058 **Fig. 6.** Photographs showing the different studied carbonate facies, which were deposited in  
1059 different sedimentary palaeoenvironments. **A-B.** Freshwater facies association. **A.** Field  
1060 photograph showing tabular black limestone interbedded with thin beds of greenish marl. Note  
1061 root traces at the top of the beds. Coin is 2.3 cm in diameter. **B.** Transmitted light  
1062 photomicrograph showing a wackestone of charophyte thalli forming the nucleus of oncoids. **C-**  
1063 **D.** Marine-influenced facies association. **C.** Field photograph showing tabular marine-influenced  
1064 black limestone. Note the root traces at the top of the bed. Tip of hammer at the top-right corner  
1065 for scale. **D.** Transmitted light photomicrograph showing a wackestone of dasycladales green  
1066 algae. **E-F.** Marginal-marine facies association. **E.** Field photograph of dolostone displaying  
1067 wavy bedding with alternation of grainy facies showing small-scale cross-bedding (red arrows)

1068 and muddy facies (blue arrows). Coin is 2.4 cm in diameter. **F.** Transmitted light  
1069 photomicrograph showing a wackestone-packstone of benthic miliolid foraminifera and  
1070 ostracods. **G-H.** Hypersaline facies association. **G.** Field photograph of hypersaline dolostone  
1071 displaying abundant calcite pseudomorphs after gypsum (yellow arrows). **H.** Transmitted light  
1072 photomicrograph showing a dolomudstone displaying calcite pseudomorphs after lenticular  
1073 gypsum.

1074 **Fig. 7. A.** Carbon and oxygen isotope compositions of carbonates of the different facies  
1075 associations in the Leza River section (Western Sector) and in the Préjano section (Eastern  
1076 Sector). In both sectors, carbonates of each facies association have negative and variable  $\delta^{13}\text{C}$   
1077 values and relatively invariant  $\delta^{18}\text{O}$  values (more negative in freshwater limestone and  
1078 progressively more positive in marginal-marine and hypersaline carbonates). **B-C.**  $\delta^{18}\text{O}$  and  
1079  $^{87}\text{Sr}/^{86}\text{Sr}$  values, respectively, *versus* the depositional environments where carbonate  
1080 precipitated in both sectors. Note that in both sectors and, as expected,  $\delta^{18}\text{O}$  values (B) are  
1081 more negative in freshwater limestone, becoming progressively heavier in marine-influenced,  
1082 marginal-marine and hypersaline carbonates. Note that most of the marine carbonates are in  
1083 the range of or close to the published  $\delta^{18}\text{O}$  values of the Barremian-Aptian marine carbonates  
1084 (see text for explanation). However,  $^{87}\text{Sr}/^{86}\text{Sr}$  ratios in each sector are very different, but  $\delta^{18}\text{O}$   
1085 values of carbonates precipitated in the different palaeoenvironments in each sector are similar.  
1086 Also note that  $^{87}\text{Sr}/^{86}\text{Sr}$  ratios in the Western Sector are similar or in the range of the published  
1087 Barremian-Aptian marine carbonates, even those obtained from freshwater carbonates.

1088

1089 **Table 1 (Supplementary material).** Isotopic data of the analysed samples

1090



Fig. 1

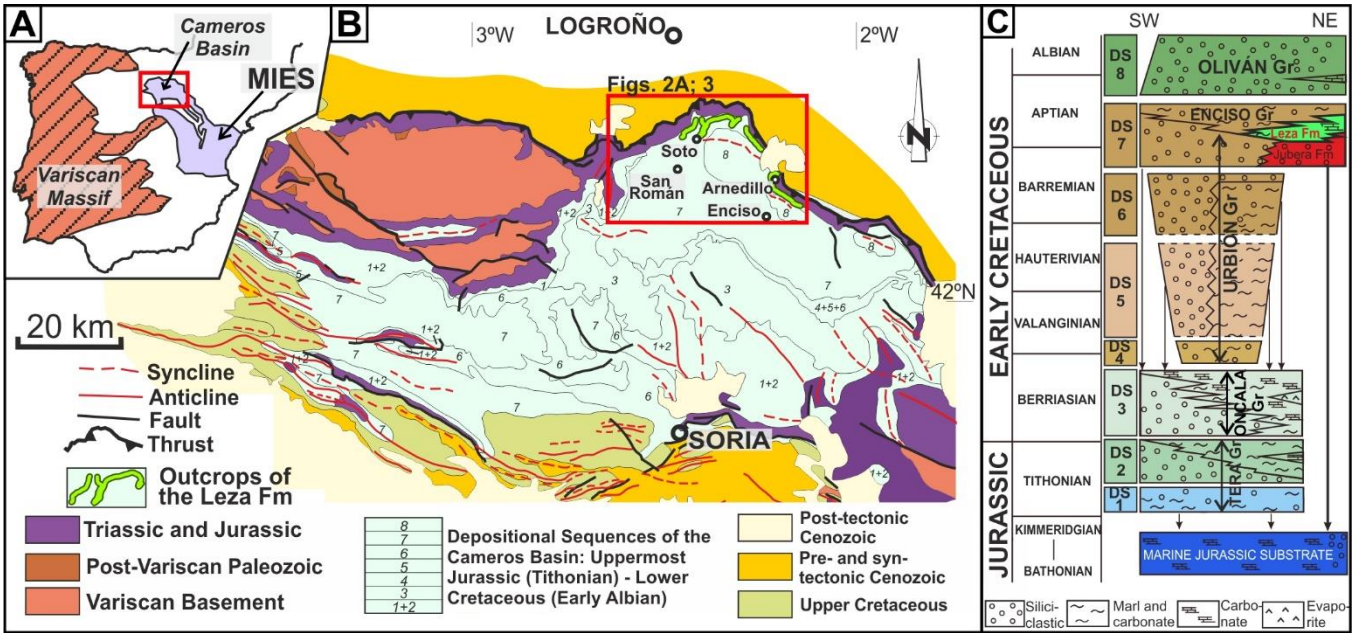


Fig. 2

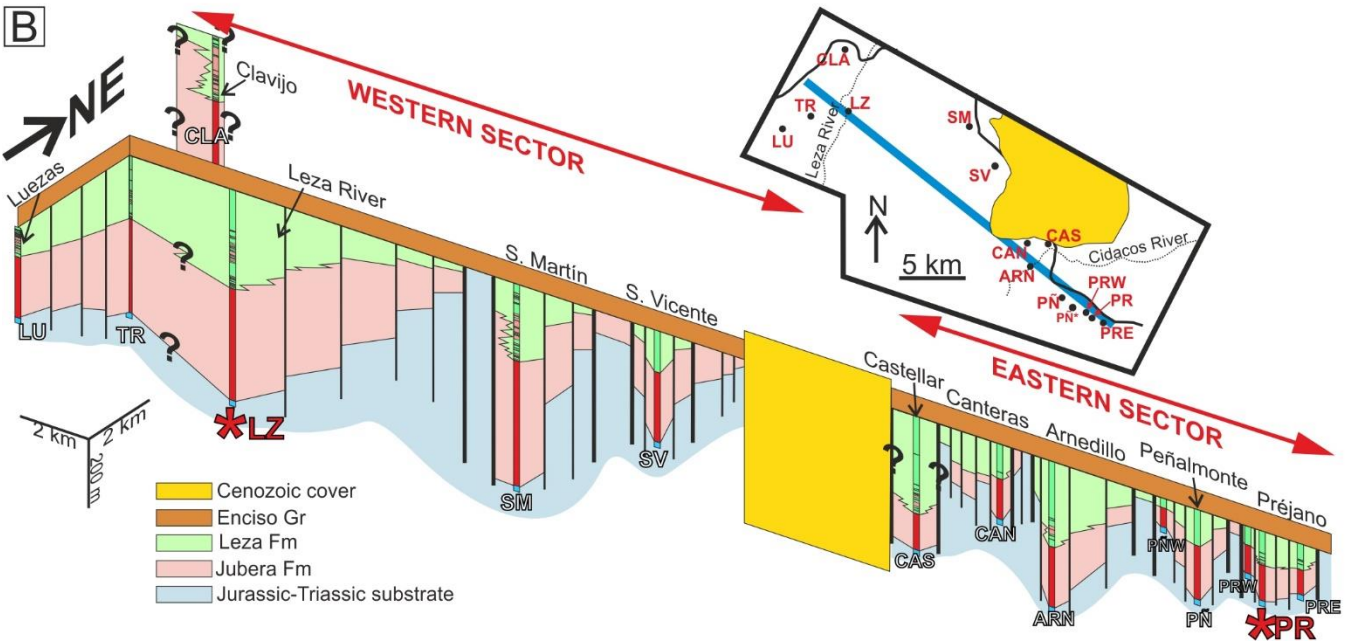
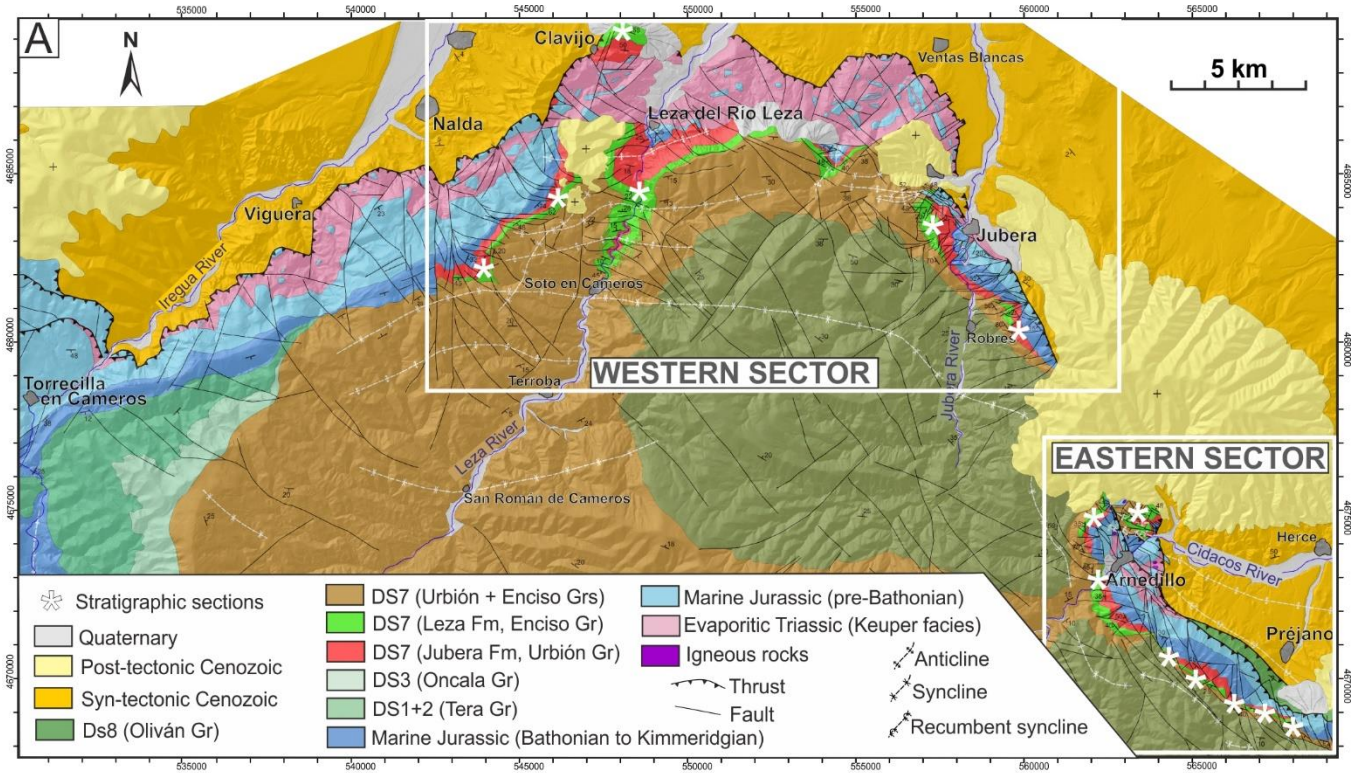


Fig. 3

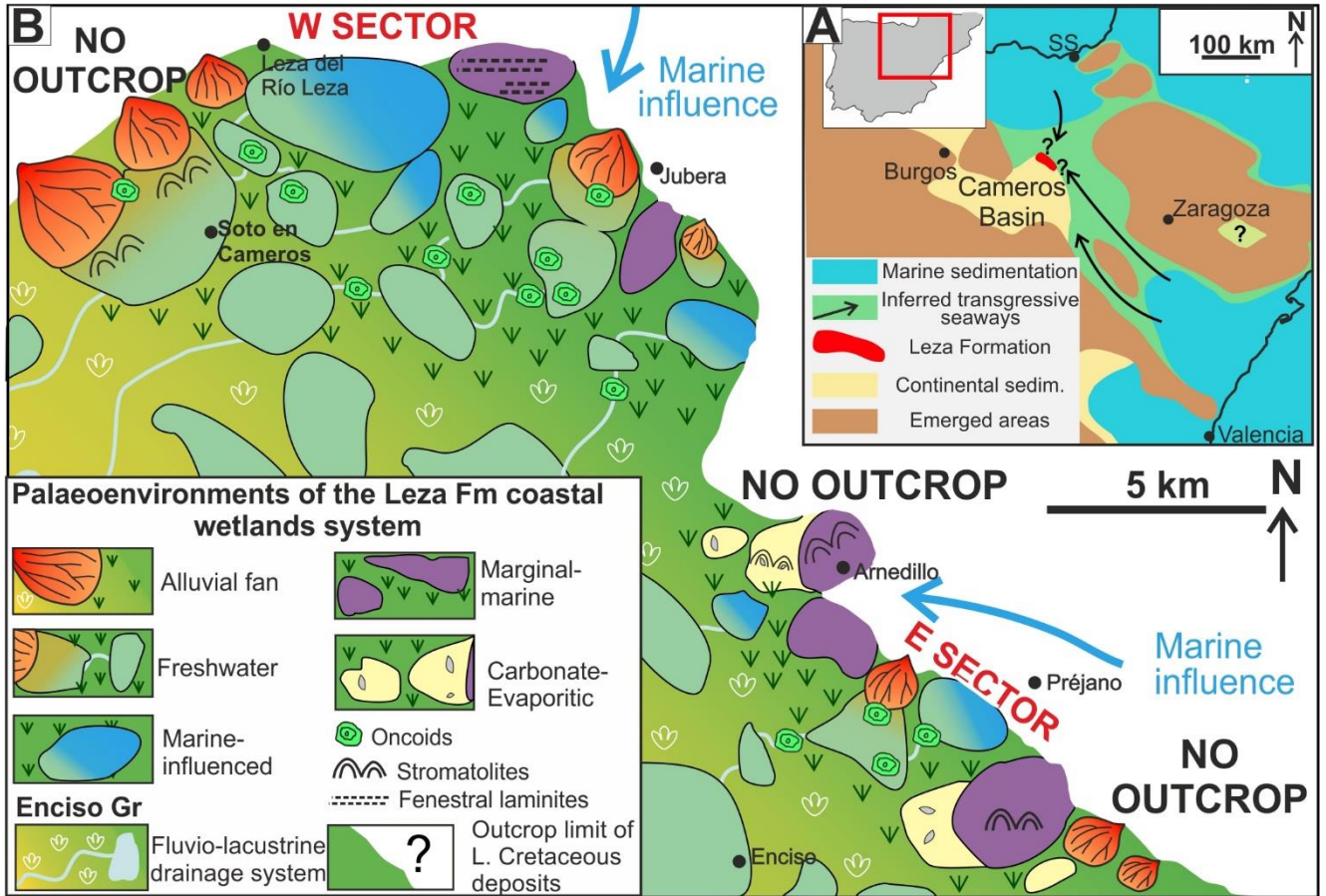


Fig. 4

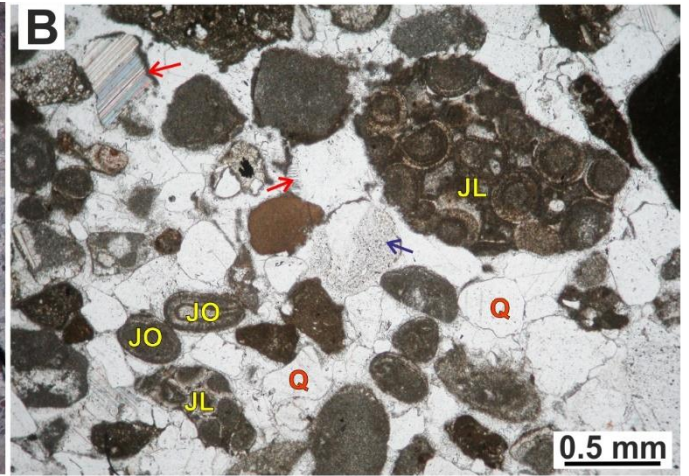
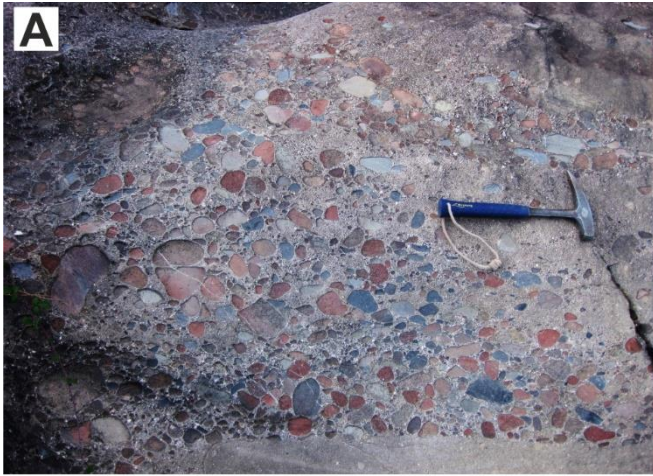


Fig. 5

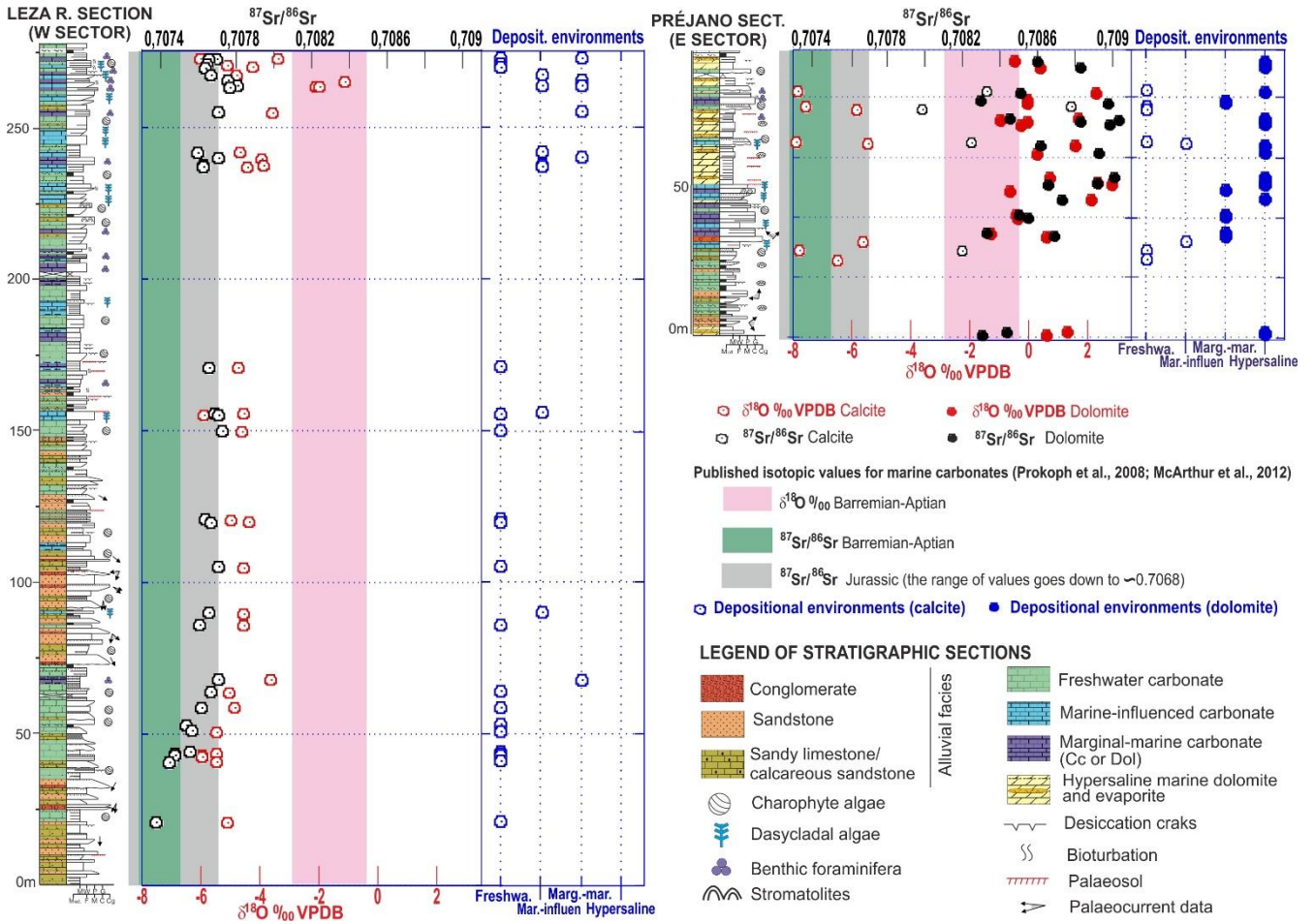


Fig. 6

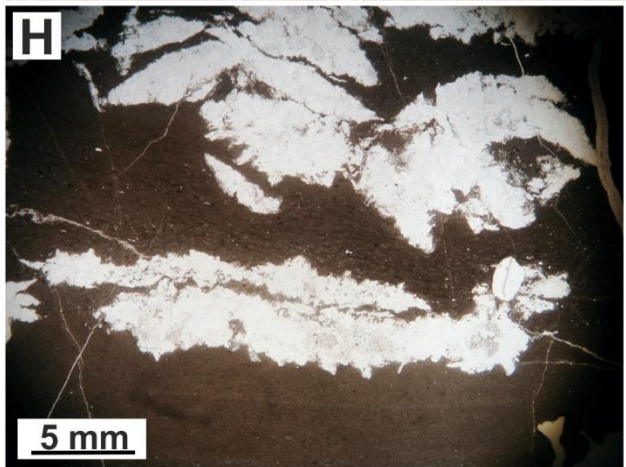
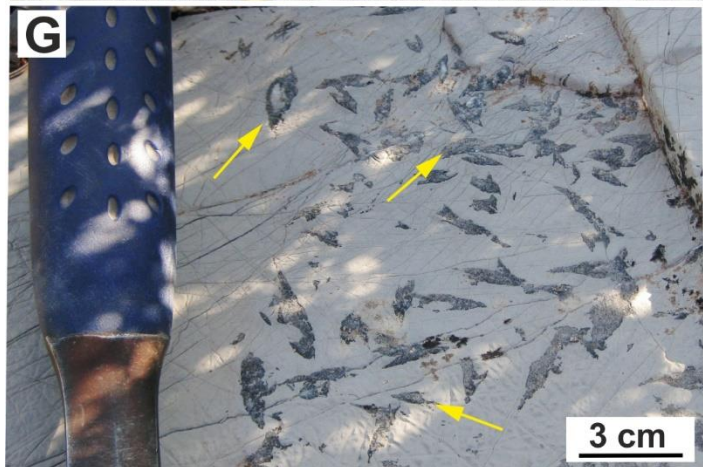
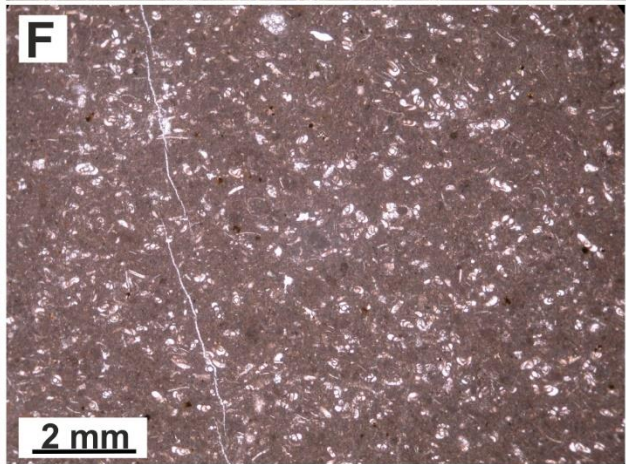
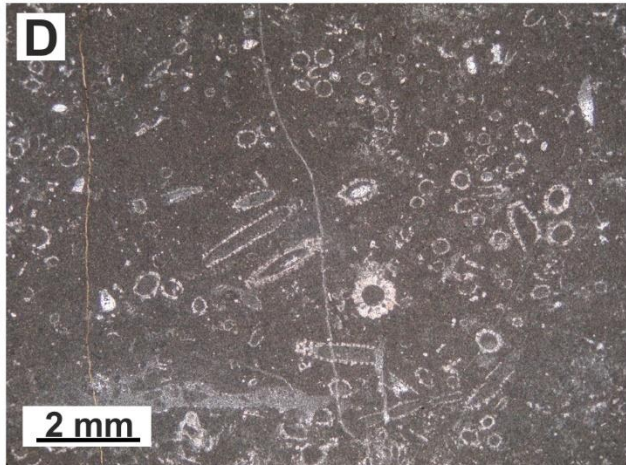
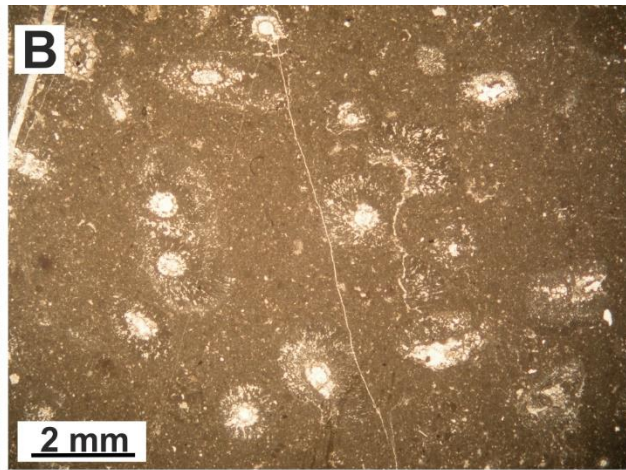


Fig. 7

